



THIS MANUSCRIPT HAS BEEN SUBMITTED TO THE JOURNAL OF GLACIOLOGY AND HAS NOT BEEN PEER-REVIEWED.

Investigating snow sinks on level sea ice: A case study in the western Arctic

Journal:	<i>Journal of Glaciology</i>
Manuscript ID	JOG-2024-0156
Manuscript Type:	Article
Date Submitted by the Author:	28-Nov-2024
Complete List of Authors:	Merkouriadi, Ioanna; Finnish Meteorological Institute, Space and Earth Observation Center Jutila, Arttu; Finnish Meteorological Institute, Earth Observation Research Liston, Glen; Colorado State University Preußer, Andreas; German Aerospace Center DLR Bonn Webster, Melinda; University of Washington
Keywords:	Sea ice, Snow, Arctic glaciology, Airborne electromagnetic soundings, Glaciological model experiments
Abstract:	We examined snow sinks on level sea ice caused by snow and sea ice interactions (snow-ice formation and sub-parcel snow mass redistribution) in the western Arctic. We coupled SnowModel-LG, a modeling system adapted for snow depth and density reconstruction over sea ice, with HIGHTSI, a 1-D thermodynamic sea ice model, to create SMLG_HS. SMLG_HS simulations of snow depth, snow-ice, and sea ice thickness were evaluated against high-resolution airborne observations from the western Arctic, highlighting the importance of snow mass changes due to snow redistribution processes. Without accounting for these processes, snow on level ice was overestimated by the model, resulting in underestimation of level ice thickness and overestimation of snow-ice thickness. In our case study, we show that snow depth on level ice needs to be reduced by up to 40% to simulate both snow and level ice thicknesses realistically in the western Arctic in April 2017. Analysis of snow volume distribution between level and deformed sea ice using

	airborne radar observations supported the model results. In addition, it revealed a linear relationship between the fraction of snow volume on level ice and the fraction of level ice along a sea ice transect in spring: $f_{Vs,level} = (0.68 \pm 0.05) f_{level}$

SCHOLARONE™
Manuscripts

Investigating snow sinks on level sea ice: A case study in the western Arctic

Ioanna MERKOURIADI,¹ Arttu JUTILA,¹ Glen E. LISTON,² Andreas PREUSSER,^{3,4} Melinda A. WEBSTER⁵

¹*Finnish Meteorological Institute (FMI), Helsinki, Finland*

²*Cooperative Institute for Research in the Atmosphere (CIARA), Colorado State University, Fort Collins, CO, USA*

³*Alfred-Wegener-Institut, Helmholtz-Zentrum für Polar- und Meeresforschung (AWI), Bremerhaven, Germany*

⁴*Present address: German Space Agency at DLR, Bonn, Germany*

⁵*Polar Science Center (PSC), Applied Physics Laboratory, University of Washington, Seattle, WA, USA*

Correspondence: Ioanna Merkouriadi <ioanna.merkouriadi@fmi.fi>

ABSTRACT. We examined snow sinks on level sea ice caused by snow and sea ice interactions (snow-ice formation and sub-parcel snow mass redistribution) in the western Arctic. We coupled SnowModel-LG, a modeling system adapted for snow depth and density reconstruction over sea ice, with HIGHTSI, a 1-D thermodynamic sea ice model, to create SMLG_HS. SMLG_HS simulations of snow depth, snow-ice, and sea ice thickness were evaluated against high-resolution airborne observations from the western Arctic, highlighting the importance of snow mass changes due to snow redistribution processes. Without accounting for these processes, snow on level ice was overestimated by the model, resulting in underestimation of level ice thickness and overestimation of snow-ice thickness. In our case study, we show that snow depth on level ice needs to be reduced by up to 40% to simulate both snow and level ice thicknesses realistically in the western Arctic in April 2017. Analysis of snow volume distribution between level and deformed sea ice using airborne radar observations supported the model results. In addition, it revealed a linear

28 **relationship between the fraction of snow volume on level ice and the fraction**
29 **of level ice along a sea ice transect in spring:** $f_{V_{s,level}} = (0.68 \pm 0.05) \times f_{level}$.

30 1 INTRODUCTION

31 Arctic sea ice is going through unprecedented changes, decreasing dramatically both in extent (e.g. Stroeve
32 and others, 2014) and in thickness (Maslanik and others, 2007; Kwok and others, 2009), and transitioning
33 from a multi-year ice to a seasonal, first-year ice system (Meier and others, 2014). The role of snow in sea ice
34 mass balance is becoming increasingly amplified in many ways, because of the higher sensitivity of sea ice
35 to its environmental conditions. The thermal resistance of snow cover significantly reduces the atmosphere-
36 ocean heat fluxes, regulating sea ice growth in winter (Maykut, 1978; Ledley, 1991). The high snow albedo
37 reflects most of the solar radiation back to space, delaying sea ice from melting in spring (Perovich and
38 others, 2017). The snow load may submerge thinner ice underneath the water level, creating negative
39 freeboard conditions (Granskog and others, 2017; Merkouriadi and others, 2020). If sea water floods at the
40 ice/snow interface and freezes there, snow-ice is formed that is a mixture of frozen seawater and snow (e.g.
41 Leppäranta, 1983), and increases the thickness of the sea ice. Snow-ice is a common phenomenon in seas
42 that are seasonally covered by ice (i.e., Baltic Sea, Sea of Okhotsk) and in large parts of the Antarctic sea
43 ice (Massom and others, 2001), but it was not commonly observed in situ in drifting Arctic sea ice until the
44 Norwegian Young Sea ICE (N-ICE2015) expedition (Granskog and others, 2017; Provost and others, 2017).
45 Snow-ice is a sink for snow, and it can positively contribute to the sea ice mass balance (Merkouriadi and
46 others, 2017, 2020), which has implications for remote sensing retrievals of sea ice thickness. Therefore, it
47 is essential to consider it for understanding sea ice mass balance, both in contemporary times in peripheral
48 seas and in future scenarios where sea ice may be thinner than present-day conditions.

49 Accounting for different snow processes is also relevant for remote sensing applications. Satellite al-
50 timetry is the most common method for monitoring sea ice thickness, providing nearly full coverage of the
51 Arctic Ocean (Laxon and others, 2003; Markus and others, 2017; Landy and others, 2022). Information
52 on the snow load on sea ice is crucial for accurate altimetry retrievals of sea ice thickness, because radar
53 and laser altimeters, in principle, measure ice or snow freeboard: the elevation of the ice or snow surface
54 from the water surface. Snow depth and density are required to convert freeboard to sea ice thickness
55 information (e.g. Laxon and others, 2003). According to Giles and others (2007), uncertainties in snow

56 depth and density contribute 48 % and 14 %, respectively, to the total error of sea ice thickness retrievals
57 from radar altimetry. A more recent study by Landy and others (2020) estimated these uncertainties at
58 11 % for snow depth and 16 % for density. Similarly, snow depth and density uncertainties were found
59 to contribute 70 % and 30–35 %, respectively, to the total error of sea ice thickness retrievals from laser
60 altimetry (Zygmuntowska and others, 2014).

61 Snow depth and density estimates used in satellite altimetry applications are often derived from snow
62 climatologies or modified versions of snow climatologies from historical observations. The most widely
63 used snow-on-sea-ice climatology is compiled from a snow depth and density data set collected mostly over
64 multi-year ice in 1954–1991 (Warren and others, 1999). In a changing Arctic sea ice system, snow conditions
65 are expected to change as well (Blanchard-Wrigglesworth and others, 2015; Webster and others, 2021), and
66 these changes are not captured by the Warren and others (1999) climatology. In addition to the long-
67 term changes, climatology overlooks the spatio-temporal differences and interannual variability of snow
68 conditions in the Arctic, which are evidently strong (Warren and others, 1999; Webster and others, 2024).
69 To account for spatiotemporal variability, efforts have focused on reanalysis-based snow depth and density
70 reconstructions (e.g. Kwok and Cunningham, 2008; Blanchard-Wrigglesworth and others, 2018; Petty and
71 others, 2018), i.e., simulations of snow depth and density evolution on sea ice. A recent contribution was
72 SnowModel-LG, a state-of-the-art Lagrangian snow evolution model (Liston and others, 2020a). Compared
73 to other reanalysis-based products, SnowModel-LG implemented Lagrangian parcel tracking and included
74 an improved representation of snow evolution physics. It has been bias-corrected and validated against a
75 wide observation framework in all seasons and yielded good agreement, especially with in situ measurements
76 (Stroeve and others, 2020).

77 SnowModel-LG explicitly resolves many snow mass sources and sinks, such as blowing snow, static-
78 surface sublimation, and melt, by performing a snow mass-budget calculation in each time step (Liston
79 and others, 2020a). However, SnowModel-LG, similarly to all the above-mentioned Arctic snow models, is
80 not coupled to a sea ice model. Therefore, it does not account for snow sinks caused by snow-ice formation.
81 Moreover, being configured over ice parcels of kilometer-scale, it does not resolve wind-driven snow mass
82 redistribution. The latter describes the tendency of snow to accumulate on the lee side of pressure ridges
83 and other roughness elements (e.g. Liston and others, 2018) as a result of snow redistribution by the wind.
84 This process results in uneven snow load over a sea ice floe (i.e., reduced snow over level ice areas and
85 increased snow over deformed ice). Because in this study we are examining level ice only, we will be

86 referring to the sub-parcel snow mass redistribution process as a snow sink.

87 This study examines snow sinks on level Arctic sea ice (snow-ice formation and sub-parcel snow mass
88 redistribution), and quantifies their effect on snow depth evolution. To investigate this, we coupled
89 SnowModel-LG with the High-Resolution Thermodynamic Sea Ice model (HIGHTSI) (Launiainen and
90 Cheng, 1998) to produce SMLG_HS. In SMLG_HS, snow-ice forms when the ice surface is depressed
91 below the water surface (negative freeboard). SMLG_HS outputs of snow depth, snow-ice and sea ice
92 thickness from 1 August 2007 until 31 July 2021 were evaluated against airborne observations in the west-
93 ern Arctic to examine and to mitigate the biases introduced when sub-parcel snow mass redistribution
94 processes are ignored.

95 2 MATERIALS AND METHODS

96 2.1 SnowModel-LG

97 SnowModel is a collection of snow distribution and snow evolution modeling tools, applicable to any
98 environment experiencing snow, including sea ice applications (Liston and Elder, 2006a; Liston and others,
99 2018). SnowModel-LG is adapted for snow depth and density reconstruction over sea ice (Liston and
100 others, 2020a). It is implemented in a Lagrangian framework to simulate snow properties on drifting sea
101 ice parcels. SnowModel-LG accounts for physical snow processes such as sublimation from static surfaces
102 and blowing snow, snow melt, evolution of snow density and temperature profiles, energy and mass transfers
103 within the snowpack, and superimposed ice formation in a multi-layer configuration. The ice parcels are
104 1-D, and they do not interact with each other.

105 At each time step (3-hour here), SnowModel-LG performs a mass-budget calculation, where snow water
106 equivalent (SWE) depth (m) is defined by snow mass gains, losses, and ice parcel dynamics,

$$107 \quad \frac{dSWE}{dt} = \frac{1}{\rho_w} [(P_r + P_s) - (S_{ss} + S_{bs} + M) + D] \quad (1)$$

108 where t (s) is time; $\rho_w = 1000 \text{ kg m}^{-3}$ is the water density; P_r ($\text{kg m}^{-2} \text{ s}^{-1}$) and P_s ($\text{kg m}^{-2} \text{ s}^{-1}$) are the
109 water-equivalent rainfall and snowfall fluxes, respectively; S_{ss} ($\text{kg m}^{-2} \text{ s}^{-1}$) and S_{bs} ($\text{kg m}^{-2} \text{ s}^{-1}$) are the
110 water-equivalent sublimation from static-surface and blowing-snow processes, respectively; M ($\text{kg m}^{-2} \text{ s}^{-1}$)
111 is the melt-related mass loss; and D ($\text{kg m}^{-2} \text{ s}^{-1}$) represents the mass losses and gains from sea ice dynamics
112 processes (i.e., parcels being created and lost with ice motion, divergence, and convergence).

113 Snow depth h_s (m) is related to SWE through the ratio of snow (ρ_s), and water (ρ_w) densities,

$$114 \quad SWE = \frac{\rho_s}{\rho_w} h_s. \quad (2)$$

115 Therefore, the evolution of snow depths and densities are calculated by

$$116 \quad \frac{d(\rho_s h_s)}{dt} = (P_r + P_s) - (S_{ss} + S_{bs} + M) + D. \quad (3)$$

117 In SnowModel-LG, snow density evolves and changes in response to compaction (weight of the above snow
118 layers), wind force, freezing of liquid water, and vapor flux through the snowpack. Additional information
119 on the components and the configuration of SnowModel-LG are summarized and provided in great detail in
120 Liston and others (2020a). The model configuration in this study is identical to the one used in Liston and
121 others (2020a), only here we have coupled it to a sea ice model (Sections 2.2–2.3). According to Stroeve
122 and others (2020), SnowModel-LG performed well in capturing the spatial and seasonal variation of snow
123 distributions, when evaluated against several Arctic data sets, including NASA Operation IceBridge (OIB),
124 ice mass balance buoys, snow buoys, MagnaProbes, and ruler measurements.

125 In the simulations presented herein, Lagrangian parcel tracking began on 1 August 2007. At the start
126 of the first simulation year, the model assumes no snow atop the sea ice, which is well supported by in situ
127 observations from the contemporary period (Radionov and others, 1997; Chapman-Dutton and Webster,
128 2024; Webster and others, 2024); the following years carry available snow from 31 July to 1 August.
129 Essential inputs are atmospheric reanalysis estimates of near-surface air temperature, relative humidity,
130 precipitation, wind speed and direction, and sea ice motion and concentration products, described in detail
131 in Section 2.4.

132 2.2 HIGHTSI

133 HIGHTSI is a 1-D thermodynamic sea ice model designed to simulate the evolution of snow and sea ice
134 thickness and temperature profiles (Launiainen and Cheng, 1998) by solving the heat conduction equation
135 for multiple ice and snow layers. The sea ice thermal conductivity is parameterized following Pringle and
136 others (2007). HIGHTSI simulates snow-ice formation following Saloranta (2000).

137 HIGHTSI has been widely used in process studies and validated extensively against observations (Cheng
138 and others, 2008b, 2013; Wang and others, 2015; Merkouriadi and others, 2017, 2020). In this study, we

139 used a model configuration that is derived from validation studies on Arctic sea ice. The model's vertical
140 resolution has been found to be critical for its performance in the Arctic (Cheng and others, 2008a).
141 Here, we used 20 layers in the ice which is considered optimal for capturing internal thermodynamic
142 processes (Cheng and others, 2008a,b, 2013; Wang and others, 2015). Detailed information on model
143 parameterizations is given in Table S1 in the supplementary material.

144 Merkouriadi and others (2020) implemented HIGHTSI in a Lagrangian framework to examine pan-
145 Arctic snow-ice distributions. In the study presented herein, HIGHTSI was modified further, so that snow
146 depth and bulk density evolution were simulated by SnowModel-LG in a 25-layer configuration. We did this
147 because SnowModel-LG provides a more advanced representation of snow physics compared to HIGHTSI's
148 snow configuration. Additionally, we wanted to explore the effects of snow sinks using a publicly available
149 snow product such as SnowModel-LG.

150 **2.3 SMLG_HS**

151 We performed two separate snow-on-sea-ice simulations. First, we simulated snow depth and density
152 with SnowModel-LG (i.e. Liston and others, 2020a). Second, SnowModel-LG's snow depth and density
153 evolution were coupled with HIGHTSI's snow-ice and thermodynamic ice growth representations. The
154 coupled output is hereafter referred to as being created by SMLG_HS.

155 For the SMLG_HS runs, snow density was simulated following Appendix C of Liston and others (2020a)
156 and stored as a bulk density value. To represent the typical snow stratigraphy of snow on Arctic sea ice (i.e.
157 high-density wind slab layer at the top, low-density depth hoar layer at the bottom), the vertical density
158 profile was parameterized as being a linear fit between densities that are 20% greater than the bulk snow
159 density of SnowModel-LG at the top of the snowpack and 20% less at the bottom of the snowpack.
160 These percentages are consistent with snow-pit measurements made during the Multidisciplinary drifting
161 Observatory for the Study of Arctic Climate (MOSAiC) expedition in 2019–2020 (Macfarlane and others,
162 2023). This approach was chosen to provide a best-possible fit to available snow density observations and
163 to account for changes in snow density in response to snow-ice formation. When snow-ice was formed, the
164 corresponding snow-depth amount was removed from the lower density bottom layers of the snowpack, and
165 the bulk density was recalculated based on the depth and density of the remaining snow. Additional model
166 specifications are presented in the supplementary material (Table S1).

167 2.4 Input Data Sets

168 Daily ice concentrations (15–100 %) by the NASA team algorithm DiGirolamo and others (2022) were
169 used to define whether an ice parcel existed and whether snow could accumulate on that parcel. Ice
170 motion vectors from Tschudi and others (2019, 2020) gridded over 25-km spatial resolution were used as
171 Lagrangian ice parcel tracks. NASA’s Modern Era Retrospective Analysis for Research and Application
172 Version 2 (MERRA-2; Global Modeling And Assimilation Office (GMAO), 2015a,b; Gelaro and others,
173 2017) was used as atmospheric forcing to SMLG_HS. Specifically, SMLG_HS was forced with 10-m wind
174 speed and direction, 2-m air temperature and relative humidity, and total water-equivalent precipitation
175 from MERRA-2. During these simulations, MicroMet (Liston and Elder, 2006b) provided the required
176 liquid and solid precipitation, and the downwelling shortwave and longwave radiation following Liston and
177 others (2020a).

178 We applied the same bias-correction in MERRA-2 reanalysis as in Liston and others (2020a), where
179 snow depth observations from NASA OIB (2009–2016) were used to scale the precipitation inputs. In
180 Liston and others (2020a), 8-year averages of precipitation scaling factors were calculated and they were
181 applied over all ice parcels and through the whole simulation period, making the results of MERRA-2 and
182 the European Centre for Medium-Range Weather Forecasts (ECMWF) ReAnalysis-5th Generation (ERA5;
183 Hersbach and others, 2020) model runs similar. Scaling factor was 1.37 for MERRA-2, indicating the need
184 to increase the precipitation inputs in order to match the OIB observations. The same scaling factor was
185 used in this study for the results to be comparable with the publicly available SnowModel-LG snow depth
186 and density data set (Liston and others, 2020b).

187 For the ocean boundary forcing, at the ice/ocean interface, we used ocean heat flux from the Ocean
188 Reanalysis System 5 (ORAS5) provided at the ECMWF (Zuo and others, 2019). ORAS5 resolution is eddy-
189 permitting (0.25° latitude and longitude) horizontally and 1 m vertically. ORAS5 includes five ensemble
190 members and covers the period from 1979 onward. In our study, we used the ensemble mean, providing
191 one unique value on a 1° grid for each simulation day.

192 2.5 Model Configuration and Outputs

193 The simulations began on 1 August 2007 and ran through 31 July 2021. Temporal resolution was 3 h to
194 capture diurnal variations, and the parcel-specific outputs (e.g. snow depth, snow bulk density, sea ice
195 thickness, and snow-ice thickness) were saved at the end of each day. Ice parcel trajectories were linearly

196 interpolated from weekly to daily time steps. On 1 August of each year (except in the first year), the
197 multi-year ice thicknesses were calculated from the sea ice thickness distribution on 31 July. The initial ice
198 thickness conditions on 1 August 2007 were defined by performing a one-year simulation with a domain-
199 wide initial condition of 1 m, and then using the ice thickness distribution at the end of the first simulation
200 year as the initial condition for the beginning of the 14-year simulation (i.e., the model ran the first year
201 twice and assumed the 31 July 2008 ice thickness distribution equaled the 1 August 2007 distribution). In
202 addition, any snow remaining at 00:00 UTC on 1 August (the last time step on 31 July) was used as the
203 initial condition for the following simulation year that started at 03:00 UTC on 1 August (these are the
204 standard model spin-up procedures as implemented in Liston and others (2020a)).

205 The daily simulation outputs for each parcel (approximately 61,000 parcels each year) were gridded
206 to the 25 km \times 25 km Equal-Area Scalable Earth (EASE) grid, provided by the National Snow and Ice
207 Data Center (NSIDC). The location of each parcel was used to calculate the overlap between that parcel
208 and the EASE grid cell, i.e. the fractional area of the EASE grid cell that was occupied by the parcel.
209 The fractional area was then multiplied by the sea ice concentration of the parcel, and the result was used
210 to weigh the parcels' contribution to each EASE grid cell. This procedure of area- and concentration-
211 weighted averages within the EASE grid cells conserved the examined parameters, similar to Liston and
212 others (2020a); Merkouriadi and others (2020).

213 2.6 Evaluation Exercise

214 To evaluate SMLG_HS snow depth and sea ice thickness, we compared them against a total of more than
215 100 airborne surveys from the Alfred Wegener Institute's (AWI) IceBird and NASA OIB campaigns over
216 the western Arctic in late winter 2009–2019 (Fig. 1). Summarizing descriptions of the respective data sets
217 are given in the Sections 2.6.1 and 2.6.2 below. We averaged the airborne measurements over the same
218 model EASE grid when more than 50 values were present in a grid cell.

219 2.6.1 AWI IceBird

220 The AWI IceBird program carried out 11 survey flights over the western Arctic Ocean in April 2017 and
221 2019, monitoring the regional sea ice conditions in very high resolution (Table 1). The nominal measurement
222 spacing along-track is 5–6 m. Snow depth data were derived from an airborne snow radar similar to OIB
223 using the Peakiness retrieval algorithm (Juttila and others, 2021a,b, 2022b). Sea ice thickness was derived

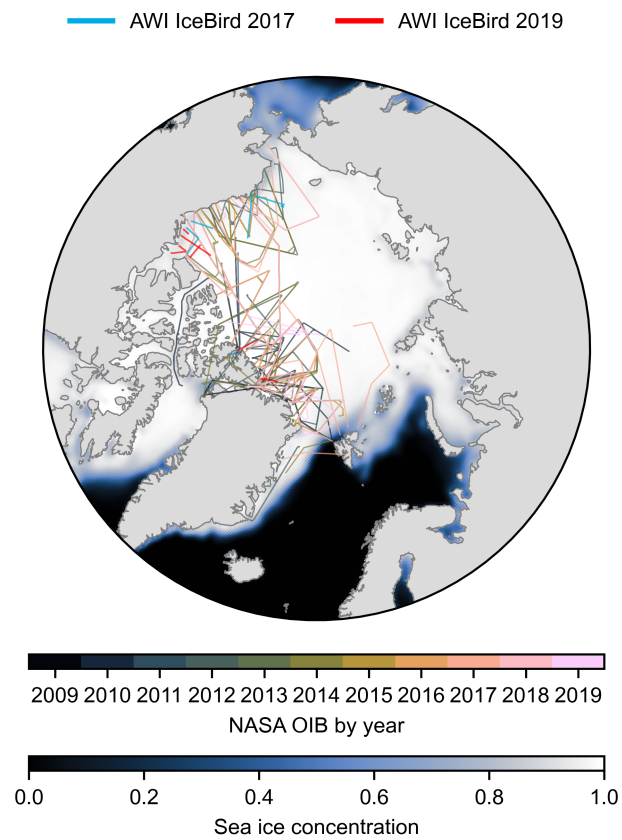


Fig. 1. Spatial and annual coverage of the 11 AWI IceBird survey flights in 2017 & 2019 (Table 1) and the 99 NASA Operation IceBridge (OIB) survey flights in 2009–2019 (Table 2 in Appendix A). The background shows the average March–April monthly sea ice concentration in 2009–2019.

Table 1. Statistics of the 11 AWI IceBird survey flights over the western Arctic Ocean in 2017 and 2019 (Fig. 1) used in this study, where L is the total length of the survey flight, $\bar{h}_{s,\text{level}}$ is the average snow depth on level ice, $\bar{h}_{s,\text{deformed}}$ is the average snow depth on deformed ice, $\bar{h}_{s,\text{all}}$ is the average snow depth of the entire survey flight including all ice types, $\frac{\bar{h}_{s,\text{level}}}{\bar{h}_{s,\text{deformed}}}$ is the fraction of the average snow depth on level ice to the average snow depth on deformed ice, f_{level} is the level ice fraction of the survey flight, $f_{V_{s,\text{level}}}$ is the fraction of snow volume on level ice, f_{MYI} is the fraction of multi-year ice (MYI), and f_{NaN} is the fraction of missing snow depth data

Date	L (km)	$\bar{h}_{s,\text{level}}$ (m)	$\bar{h}_{s,\text{deformed}}$ (m)	$\bar{h}_{s,\text{all}}$ (m)	$\frac{\bar{h}_{s,\text{level}}}{\bar{h}_{s,\text{deformed}}}$	f_{level}	$f_{V_{s,\text{level}}}$	f_{MYI}	f_{NaN}
2017-03-30	374		N/A ^a	0.327			N/A ^a		0.527
2017-04-02 ^b	415	0.213	0.300	0.265	0.709	0.397	0.319	0.000	0.231
2017-04-04 ^b	266	0.158	0.233	0.200	0.677	0.439	0.346	0.000	0.231
2017-04-06 ^b	460	0.133	0.199	0.176	0.666	0.342	0.257	0.000	0.228
2017-04-08	619	0.080	0.162	0.136	0.490	0.323	0.189	0.000	0.308
2017-04-10	49		N/A ^a	0.226			N/A ^a		0.627
2019-04-02	408	0.361	0.377	0.375	0.956	0.128	0.123	0.808	0.446
2019-04-05	187	0.120	0.329	0.298	0.364	0.148	0.059	0.778	0.243
2019-04-07	470	0.069	0.211	0.160	0.328	0.363	0.157	0.183	0.491
2019-04-08	277	0.044	0.090	0.074	0.489	0.355	0.212	0.000	0.372
2019-04-10	415	0.080	0.216	0.166	0.371	0.369	0.178	0.219	0.256
min	49	0.044	0.090	0.074	0.328	0.128	0.059	0.000	0.228
mean	358	0.140	0.235	0.218	0.561	0.318	0.205	0.221	0.360
max	619	0.361	0.377	0.375	0.956	0.439	0.346	0.808	0.627

^aNot applicable; no sea ice thickness measurements

^bUsed in the sensitivity experiment (Section 2.7)

224 by subtracting snow depth from the total (sea ice + snow) thickness data measured simultaneously with
 225 a towed electromagnetic sounding instrument (Jutilla and others, 2022a; Jutilla and others, 2024a,b). We
 226 distinguished measurements over level ice by using the flag in the data product that implements a sea ice
 227 thickness gradient threshold of 4 cm within an along-track distance of 1 m over continuous sections of at
 228 least 100 m long.

229 2.6.2 NASA OIB

230 Annual NASA OIB campaigns over the western Arctic Ocean took place in March–April 2009–2019 (Mac-
 231 Gregor and others, 2021) and comprise 99 survey flights in total (Table 2 in Appendix A). We used the

232 data products of Kurtz and others (2015, 2016) where the snow depth data were derived from airborne
233 snow radars using the retrieval algorithms described in Kurtz and Farrell (2011); Kurtz and others (2013).
234 The data are averaged in the along-track direction to a 40 m length scale. We did not use the OIB sea
235 ice thickness to evaluate modeled sea ice thickness, because it is not directly measured but converted from
236 freeboard and snow depth measurements assuming hydrostatic equilibrium. However, we did use it together
237 with surface roughness data included in the product to guide a level ice identification similar to the IceBird
238 data (Juttila and others, 2022a). To compensate for the increased uncertainty of sea ice thickness and the
239 multiple times coarser along-track resolution compared to the IceBird data, we applied here more strict
240 conditions including a sea ice thickness gradient threshold of 2 cm m^{-1} over continuous sections of at least
241 200 m long as well as ensuring a corresponding surface roughness value of less than 0.3 m. We determined
242 the numerical values of these conditions through manual iteration and visually inspecting along-track sea
243 ice transect profiles.

244 2.7 Sensitivity Experiment

245 Arctic sea ice floes are a mix of level and deformed ice features that affect the meter-scale spatial distribution
246 of snow properties. However, most snow models, such as SnowModel-LG, consider snow properties to be
247 evenly distributed within grid cells of a given size (e.g., $25 \text{ km} \times 25 \text{ km}$). Therefore, by not considering the
248 sub-grid distribution of snow properties, they are expected to overestimate snow thickness over level ice and
249 underestimate it over deformed ice (Sturm and others, 2002; Webster and others, 2015; Itkin and others,
250 2023). We hypothesized that SMLG_HS would overestimate snow depth on level ice, and consequently
251 underestimate level ice thickness and overestimate snow-ice thickness demonstrating the effect of sub-parcel
252 snow mass redistribution processes.

253 To test our hypothesis, we performed a modeling sensitivity experiment, where we decreased snow
254 depth in SMLG_HS by 10 % intervals. We derived a snow depth fraction that resulted in best fitting of
255 both snow depth and level ice thickness simulations to the observations. We argue that this snow depth
256 decrease represents the sub-parcel snow mass redistribution process.

257 As an independent evaluation, we investigated the snow mass redistribution between level and deformed
258 ice also along the 100+ airborne surveys in 2009–2019 by calculating the fraction of snow volume on level

ice for each flight:

$$V_{s,tot} = V_{s,level} + V_{s,deformed} = \bar{h}_{s,level} \times f_{level} + \bar{h}_{s,deformed} \times (1 - f_{level}), \quad (4a)$$

$$f_{V_{s,level}} = \frac{V_{s,level}}{V_{s,tot}} = \frac{\bar{h}_{s,level} \times f_{level}}{V_{s,tot}}, \quad (4b)$$

where $V_{s,tot}$ is the total snow volume, $V_{s,level}$ is the snow volume on level ice, $V_{s,deformed}$ is the snow volume on deformed ice, $\bar{h}_{s,level}$ is the average snow depth on level ice, $\bar{h}_{s,deformed}$ is the average snow depth on deformed ice, f_{level} is the level ice fraction, and $f_{V_{s,level}}$ is the fraction of snow volume on level ice.

3 RESULTS

In the evaluation exercise, we compared SMLG_HS simulations of snow depth and sea ice thickness against independent airborne observations from the IceBird and OIB campaigns, and we were able to examine snow depth on level ice separately. The results of the evaluation exercise confirmed our hypothesis. They indicated that SMLG_HS overestimated snow depth over level ice on average by 0.06–0.07 m with a root-mean-square error (RMSE) of 0.10–0.11 m, but with an absolute error up to 0.45 m (Figs. 2a–d and Fig. 3a–b). For comparison, in the SMLG the maximum absolute error was even higher, 0.60 m. Therefore, SMLG_HS underestimated level ice thickness on average by 0.45 m with an RMSE of 0.62 m, but with an absolute error up to 1.76 m (Figs. 2e–h and Fig. 3e). This result was consistent in all IceBird flights examined in the evaluation exercise.

When we did not distinguish between level and deformed ice and we evaluated SMLG_HS simulations against the total snow depth observations instead (over all ice types), SMLG_HS demonstrated better fit to the snow depth observations from both IceBird and OIB flights (Figs. 2a–d), with reduced RMSEs and biases compared to SMLG (Fig. 3c–d). This is an important result, because it indicates that total snow-on-sea-ice amounts given by SMLG_HS are realistic, but they do not account for the sub-grid spatial variations of snow depth (25 km × 25 km). Without considering the sub-grid snow distribution, SMLG_HS overestimated snow depth on level ice resulting in thinner level ice thickness that is more prone to snow-ice formation. The question now becomes: how much snow is lost from the level ice due to snow mass redistribution?

We examined two different approaches to address the question above and to assess the sub-parcel snow mass redistribution: (1) by conducting a modeling sensitivity experiment with a subset of IceBird flights

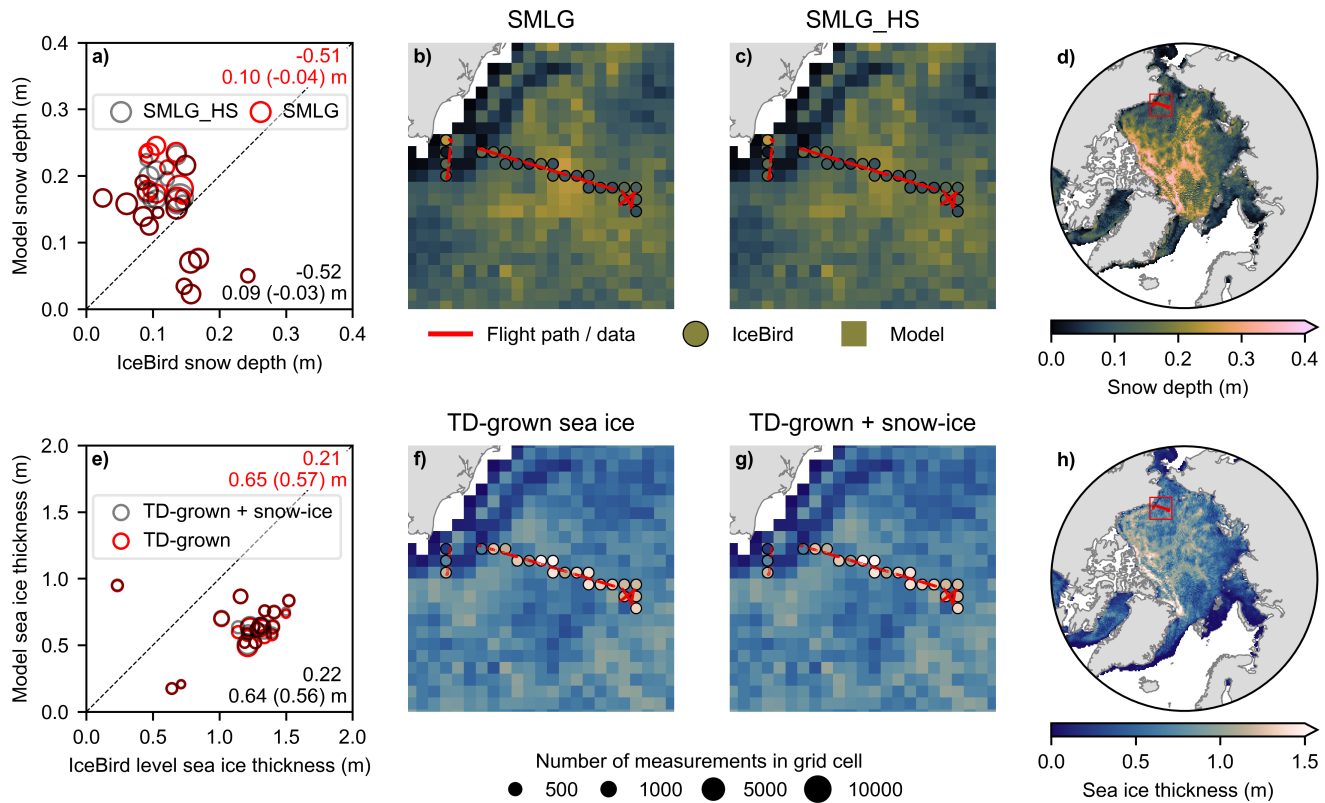


Fig. 2. Panels a)–d) show the evaluation of modeled snow depth from SMLG and SMLG_HS against airborne radar-derived snow depth measurements from the AWI IceBird survey flight on 8 April 2017. Red color refers to the original SMLG and black color to the new, coupled SMLG_HS. Panels e)–h) show the evaluation of thermodynamically-grown (TD-grown) sea ice and snow-ice modeled with SMLG_HS against airborne sea ice thickness measurements over level ice from the same flight. The red square in panels d) and h) show the extent of panels b), c), f) and g). Red color refers to only thermodynamically-grown (TD-grown) sea ice, black color indicates the sum of TD-grown sea ice and snow-ice, i.e. total sea ice thickness. In panels a) and e), the size of the data point reflects the relative number of airborne measurements in the grid cell. Upper and lower right corners of each panel show the statistics of the corresponding year: Pearson correlation coefficient r , root-mean-square error (RMSE), and lastly mean bias in parenthesis.

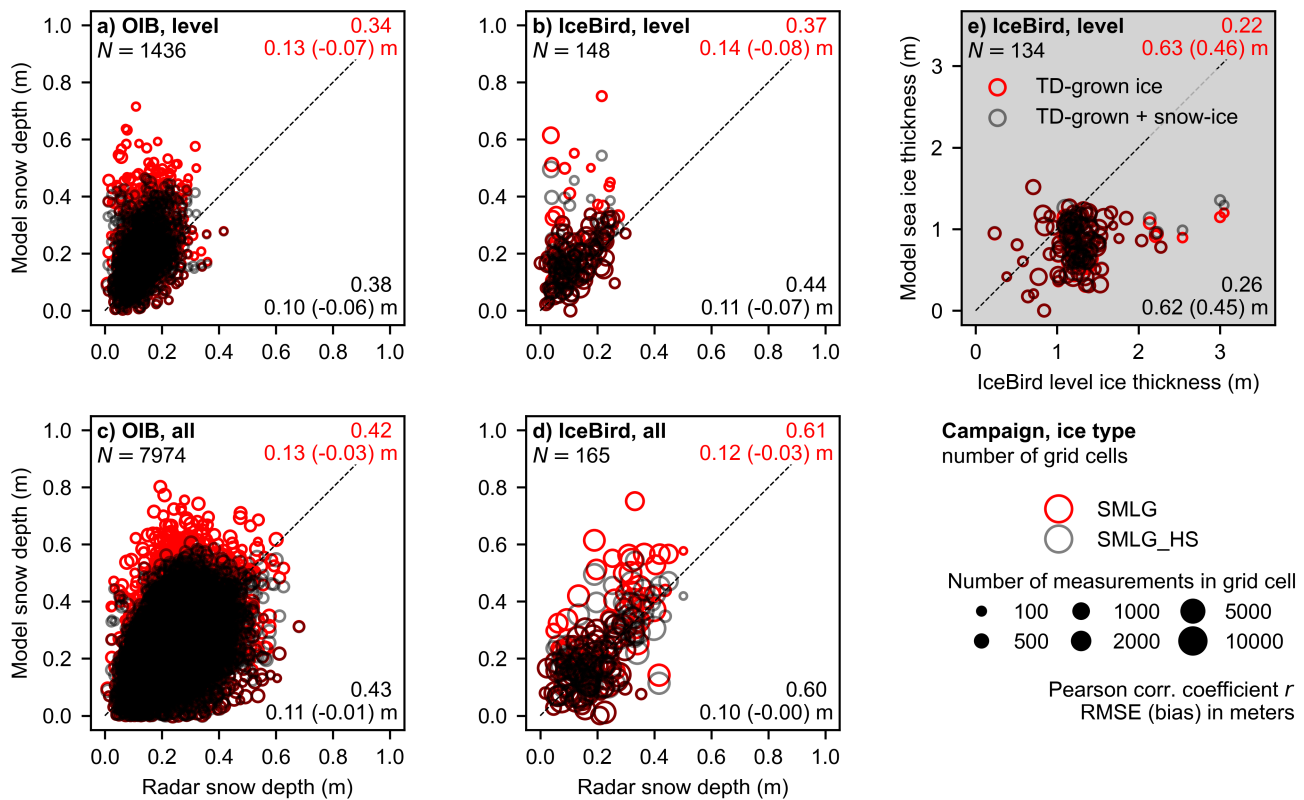


Fig. 3. Evaluation of the simulations compared against gridded airborne measurements. Panels a)–d) with white background show the modeled snow depth against radar-derived snow depth. The upper panels a)–b) show only measurements over level ice and the lower panels c)–d) show measurements over all ice types. The left-side panels a) & c) show the NASA Operation IceBridge (OIB) flights in 2009–2019 and the middle panels b) & d) show the AWI IceBird flights in 2017 & 2019. Red color refers to the original SMLG and black color to the new, coupled SMLG_HS. The upper right panel e) with grey background shows the modeled sea ice thickness compared against gridded airborne sea ice thickness measurements over level ice from the AWI IceBird campaigns in 2017 & 2019. Red color refers to only thermodynamically-grown (TD-grown) sea ice, black color indicates the sum of TD-grown sea ice and snow-ice, i.e. total sea ice thickness. The size of the data point reflects the relative number of airborne measurements in the grid cell. Upper and lower right corners of each panel show the statistics of the corresponding year: Pearson correlation coefficient r , root-mean-square error (RMSE), and lastly mean bias in parenthesis.

and (2) by performing an analysis of snow volume distribution between level and deformed sea ice based on all IceBird and OIB flight transects. The results of the modeling sensitivity experiment revealed that snow depth on level ice should be reduced by at least 40 % to simulate level ice thickness realistically and, at the same time, to maintain snow depth and sea ice thickness within their respective measurement uncertainties of 0.05 m and 0.12 m for the western Arctic in April 2017 (Fig. 4). This reduced the mean bias in level sea ice thickness by 53 % from 0.30 m to 0.14 m. The analysis of snow volume distribution along all the OIB and IceBird flight transects in 2009–2019 revealed a relationship between the fraction of level ice (f_{level}) along a sea ice transect and the fraction of snow volume on level ice ($f_{V_{s,\text{level}}}$), demonstrating the effect of the sub-parcel snow mass redistribution (Fig. 5). This relationship is linear for fractions of level ice up to 0.5, and it can be given by

$$f_{V_{s,\text{level}}} = (0.68 \pm 0.05) \times f_{\text{level}}, \quad (5)$$

where ± 0.05 represents the 95 % confidence interval of the slope.

4 DISCUSSION

We performed a modeling study to investigate snow sinks on level ice in the western Arctic. We coupled SnowModel-LG snow depth and density evolution with HIGHTSI thermodynamic sea ice and snow-ice growth to create SMLG_HS. Being in fact a 1-D model, SMLG_HS considers level ice only and assumes that negative freeboard will lead to snow-ice formation. It does not account for dynamic ice thickening, nor for sub-parcel snow mass redistribution processes, i.e., the preference of snow to accumulate over ice deformations (Liston and others, 2018). Therefore, it is expected to overestimate snow depth on level ice. Being a very effective insulator, this additional snow decelerates level ice growth, resulting in underestimation of level ice thickness and overestimation of snow-ice thickness. This hypothesis was confirmed when we compared SMLG_HS simulations to airborne observations of snow depth over level ice and level ice thicknesses. SMLG_HS did, however, match the overall snow depth observations from airborne radars better compared to SMLG, with reduced root-mean-square-errors and biases.

AWI IceBird data are ideal for evaluating SMLG_HS, because they offer simultaneous snow depth and sea ice thickness observations over hundreds of kilometers of transects in high resolution, with a possibility to examine level and deformed ice conditions separately. However, IceBird campaigns that provide a concrete data set of both snow depth and sea ice thickness observations are limited to the western Arctic

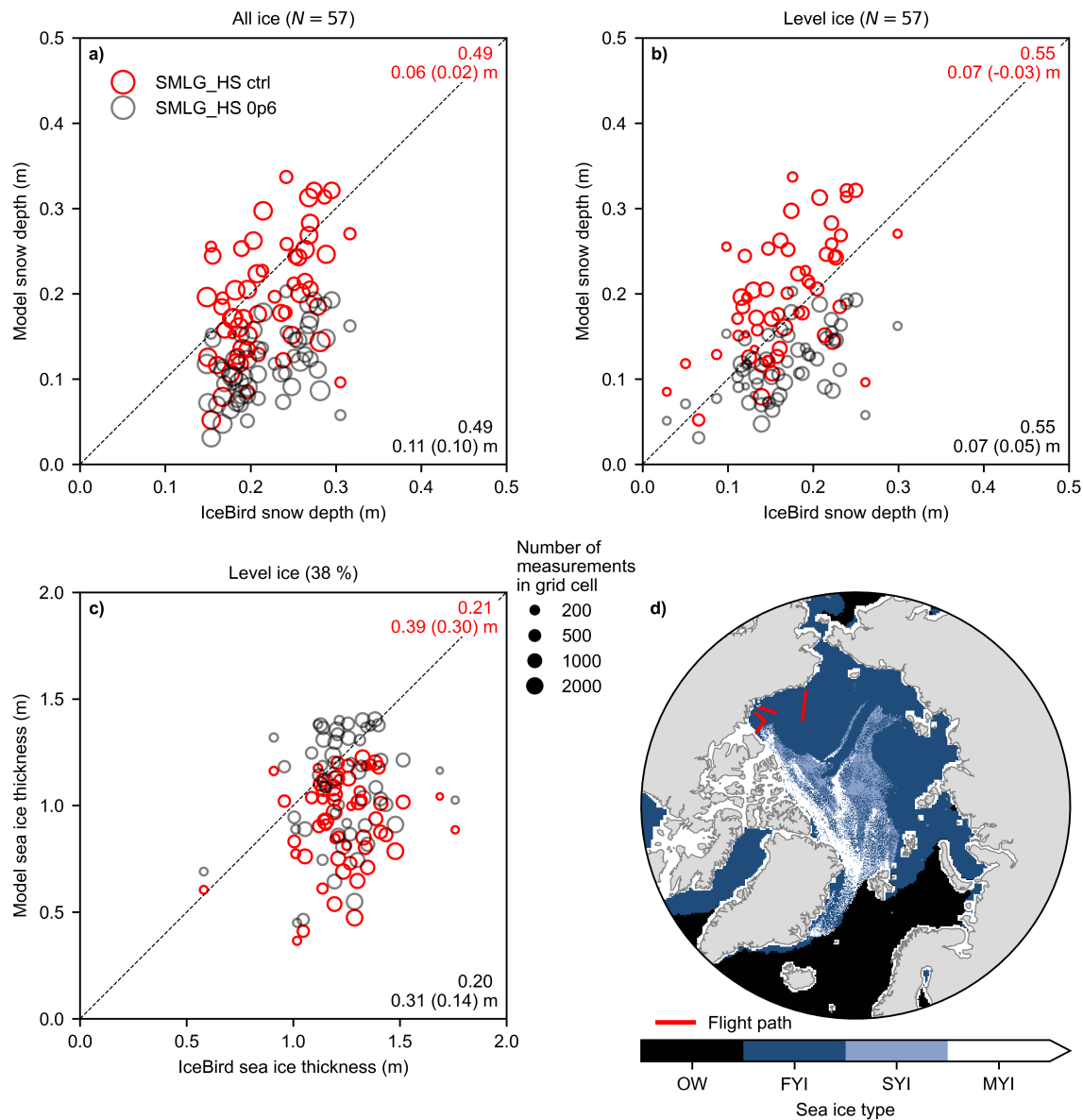


Fig. 4. Results of the sensitivity experiment showing a) snow depth over all (level and deformed) ice types, b) snow depth over level ice only, c) sea ice thickness over level ice, and d) location of the three IceBird flights (red lines; Table 1) together with the sea ice type in April 2017 at the time of the flights. The control simulation with unmodified snow depth (SMLG_HS ctrl) is shown as red circles and the simulation with snow depth reduced by 40% (SMLG_HS 0p6) as black circles. The size of the data point reflects the relative number of airborne measurements in the grid cell. While 38% of the total data are from the level ice, the total number of the grid cells ($N = 57$) is not reduced. Upper and lower right corners of panels a)–c) show the statistics of the data sets: the number above is the Pearson correlation coefficient r , while below are the root-mean-square error and lastly mean bias in parenthesis. OW stands for open water, FYI for first-year ice, SYI for second-year ice (i.e. sea ice that has survived one melt season), and MYI for multi-year ice (i.e. sea ice that has survived at least two or more melt seasons).

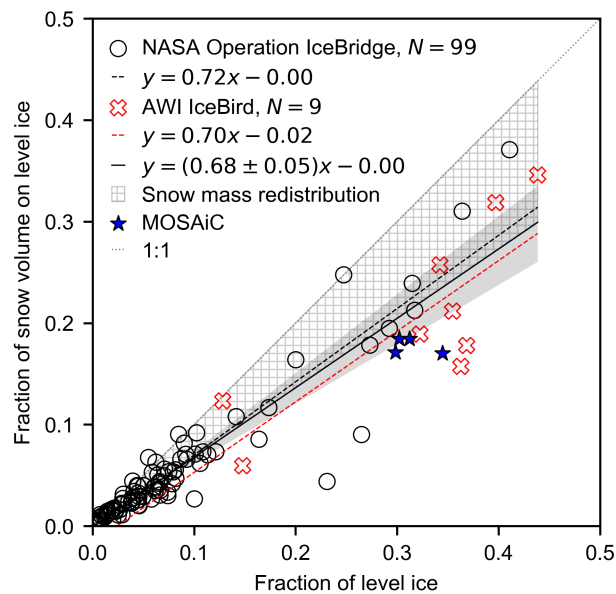


Fig. 5. The relationship between the fraction of level ice and the fraction of snow volume on level ice demonstrating the effect of snow mass redistribution (grey hatching). The NASA OIB survey flights are marked with black circles and their linear fit with a black dashed line, whereas the AWI IceBird ones are shown with red crosses and a red dashed line. The solid black line shows the linear fit of all airborne data and the grey shading is its 95% confidence interval. The blue stars show the corresponding end-of-winter values in March–April 2020 from the MOSAiC expedition ground-based transect by Itkin and others (2023).

315 and in April 2017 and 2019 only. In 2019, IceBird flew over multi-year ice that was heavily deformed,
316 resulting in small fractions of level ice along the flight tracks. The limited level ice observations would
317 impose a risk of unreliable conclusions, therefore we focused our analysis on flights with the largest level
318 ice fraction in 2017. Moreover, the monitored region was occasionally close to the coast where parcel
319 trajectory data are unavailable, rendering these regions outside the simulation domain and the sensitivity
320 experiment.

321 The modeling sensitivity experiment showed that reducing snow depth by 40 % produced the best
322 agreement between snow depth (on level ice) and level ice thickness in the western Arctic in April 2017
323 and reduced the mean bias in sea ice thickness by 53 %. The analysis of the snow volume distribution
324 between level and deformed sea ice using observations from the IceBird and OIB transects was in good
325 agreement with the model results when considering their respective limitations. The sensitivity experiment
326 relies on a 1-D thermodynamic model that does not account for lateral conduction of heat, a factor that
327 becomes significant when snow depth varies spatially (Clemens-Sewall and others, 2024; Zampieri and
328 others, 2024). Regarding the airborne approach, it is not possible to account for snow sinks in snow-ice
329 formation. Omitting snow-ice formation, that mostly occurs over level ice, would result in underestimation
330 of the snow mass redistribution.

331 We argue that the snow depth decrease on level ice represents the sub-parcel snow mass redistribution
332 process; however, this mechanism is not yet fully understood. The deformation rate of a sea ice floe, together
333 with the atmospheric conditions (e.g. wind, warm intrusions) and the properties of snow cover (density,
334 wetness, sintering level, and snow-surface shear strength) are expected to affect the snow redistribution,
335 i.e., the amount of snow removed from the level to deformed ice. Ice and snow conditions are not uniform
336 across the Arctic Ocean, but they vary regionally and temporally. Therefore, a 40 % reduction of snow
337 depth on level ice is empirical and more data is needed across the Arctic and the different seasons to study
338 the spatiotemporal variability of snow mass redistribution. In another, yet more local example by Itkin
339 and others (2023), data from the MOSAiC expedition indicated that 31 % of level ice contained only 18 %
340 of the snow volume at the end of spring (see the blue stars in Fig. 5). In the Surface Heat Budget of the
341 Arctic Ocean (SHEBA) study in 1997–1998, snowdrifts associated with ridges occupied between 3 % and
342 6 % of the total study area. The drift sections had mean depths that were on average 30 % higher than the
343 surrounding snow (Sturm and others, 2002).

344 Although the snow depth reduction suggested by the sensitivity experiment cannot be generalized across

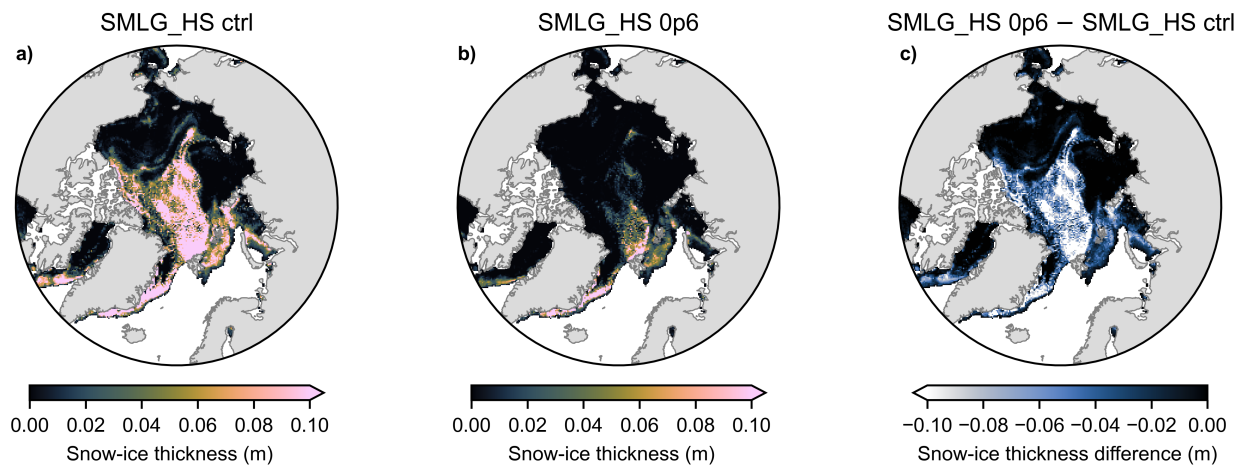


Fig. 6. Snow-ice thickness, 14-year average over the day of maximum snow-on-sea-ice volume in 2007–2021, from a) the control run (SMLG_HS ctrl), b) the run with snow depth reduced by 40% (SMLG_HS 0p6), and c) the difference between the two simulations (reduced minus control).

345 the entire Arctic and across different years, as an illustrative attempt, we compared snow-ice formation
 346 results from the SMLG_HS simulation spanning the years 2007–2021, with and without a 40% decrease
 347 in snow depth. The 14-year average snow-ice thickness on the day of maximum snow-on-sea-ice volume is
 348 shown in (Fig. 6). Even with a 40% decrease in snow depth, snow-ice still has the potential to form and is
 349 characterized by strong seasonal and regional variations. However, 40% less snow on level ice would greatly
 350 limit snow-ice formation in the central and western Arctic. This process would be primarily restricted to the
 351 Atlantic sector of the Arctic, particularly along Greenland’s east coast and north of Svalbard underneath
 352 the North Atlantic storm track, where the N-ICE2015 campaign was conducted. Snow-ice formation has
 353 also been observed with autonomous sea ice mass balance buoys similar to Provost and others (2017) (Text
 354 S2 and Fig. S1 in the supplementary material) and in fully coupled climate models (Webster and others,
 355 2021) in these regions in the contemporary period. Understanding the importance of sub-parcel snow mass
 356 redistribution will guide the development of necessary modeling tools that capture snow sinks properly.

357 5 CONCLUSIONS

358 We showed that a 1-D sea ice and snow thermodynamic model approach would overestimate snow sink in
 359 snow-ice formation. Even though the total snow depth (over both deformed and level ice) matched well
 360 with both OIB and IceBird observations, not accounting for snow redistribution from level to deformed

ice resulted in overestimation of snow depth over level ice. As expected, this additional snow decelerated thermodynamic ice growth in the model, resulting in thinner level ice that is more prone to snow-ice formation. Based on the evaluation of our simulations against IceBird data in April 2017, fitting both snow on level ice and level ice thickness simulations to the IceBird observations, snow depth in SMLG_HS should be reduced by 40%. We argue that in our 2017 case study in the western Arctic, 40% reduction in snow depth over level ice represented the sub-parcel snow mass redistribution process. Based on the analysis of more than 100 airborne survey flights spanning a full decade, the fraction of snow volume on level ice in spring is linearly related to the level ice fraction, and it is given by $f_{V_{s,level}} = (0.68 \pm 0.05) \times f_{level}$.

When snow models do not account for snow sinks caused by snow and sea ice interactions, such as snow-ice formation or sub-parcel snow mass redistribution processes, they overestimate snow depth on level ice. Uneven snow-on-sea-ice load within a sub-grid area will result in biases in altimetry retrievals of sea ice thickness by overestimating level ice and underestimating deformed ice thickness. Regarding sea ice modeling applications, spatial variability in snow depth will impact sea ice thermodynamic growth in winter, affecting both vertical and horizontal heat fluxes, and will influence melt pond formation in summer (Thielke and others, 2023). Therefore, snow-on-sea-ice reconstructions should be used with caution depending on the application requirements. This study emphasizes the need to account for sub-grid scale heterogeneity in snow and sea ice interactions to improve the representation of snow in remote sensing and model studies. It also highlights the crucial need for additional independent but simultaneous observations of snow depth and sea ice thickness, together with information on snow properties, to understand the mechanism behind snow mass changes due to coupled physical processes.

SUPPLEMENTARY MATERIAL

The supplementary material for this article can be found at... [LINK]

DATA

Model input

Sea ice concentration data are available at DiGirolamo and others (2022). Sea ice motion vectors are available at Tschudi and others (2019). Atmospheric forcing data are available at Global Modeling And Assimilation Office (GMAO) (2015a,b). Daily ocean heat flux data (opa0/daily_r1x1) were downloaded

388 from ECMWF via the ECMWF ECGATE Class Service (ECS) computing facility using Teleport SSH and
389 a personal ECMWF user account.

390 **Evaluation**

391 Airborne data are available at Jutila and others (2021a,b); Jutila and others (2024a,b) for AWI IceBird
392 and at Kurtz and others (2015, 2016) for NASA OIB. Data for SIMBA buoys are available at Preußner and
393 others (2024).

394 **ACKNOWLEDGEMENTS**

395 IM was supported by the ESA grant CCI+ 4000126449/19/I-NB. IM and AJ were supported by the
396 Research Council of Finland grant 341550. GEL was supported by the United States National Science
397 Foundation grant 1820927. AP was supported by the European Union's Horizon 2020 research and innova-
398 tion programme under grant 101003472. The authors are grateful to Bin Cheng for providing the software
399 code for the model HIGHTSI and to Polona Itkin for sharing the MOSAiC ground-based transect data.
400 Autonomous sea ice measurements (temperature profile and heating cycle data) from 2012 to 2020 were
401 obtained from <https://www.meereisportal.de> (grant: REKLIM-2013-04). The scientific colour maps
402 (Crameri, 2023) are used in this study to prevent visual distortion of the data and exclusion of readers
403 with colour-vision deficiencies (Crameri and others, 2020).

404 **FINANCIAL SUPPORT**

405 XXX

406 **AUTHOR CONTRIBUTIONS**

407 **Conceptualization:** IM. **Data curation:** IM, AJ, GEL, AP. **Formal analysis:** IM, AJ. **Funding ac-**
408 **quisition:** IM. **Investigation:** IM, AJ. **Methodology:** IM, GEL. **Project administration:** IM. **Re-**
409 **sources:** IM. **Software:** GEL. **Supervision:** IM. **Validation:** IM, GEL. **Visualization:** AJ. **Writing**
410 **— original draft:** IM. **Writing — review & editing:** IM, AJ, GEL, AP, MAW. Author contributions
411 follow the Contributor Role Taxonomy (CRediT) (Brand and others, 2015; National Information Standards
412 Organization (NISO), 2022).

413 REFERENCES

- 414 Blanchard-Wrigglesworth E, Farrell SL, Newman T and Bitz CM (2015) Snow cover on Arctic sea ice in observations
415 and an Earth System Model. *Geophysical Research Letters*, **42**, 10342–10348 (doi: 10.1002/2015GL066049)
- 416 Blanchard-Wrigglesworth E, Webster MA, Farrell SL and Bitz CM (2018) Reconstruction of Snow on Arctic Sea Ice.
417 *Journal of Geophysical Research: Oceans*, **123**, 3588–3602 (doi: 10.1002/2017JC013364)
- 418 Brand A, Allen L, Altman M, Hlava M and Scott J (2015) Beyond authorship: attribution, contribution, collabora-
419 tion, and credit. *Learned Publishing*, **28**(2), 151–155 (doi: 10.1087/20150211)
- 420 Chapman-Dutton HR and Webster MA (2024) The Effects of Summer Snowfall on Arctic Sea Ice Radiative Forcing.
421 *Journal of Geophysical Research: Atmospheres*, **129**(14) (doi: 10.1029/2023jd040667)
- 422 Cheng B, Vihma T, Zhanhai Z, Zhijun L and Huiding W (2008a) Snow and sea ice thermodynamics in the Arctic:
423 Model validation and sensitivity study against SHEBA data. *Advances in Polar Science*, **19**, 108–122
- 424 Cheng B, Zhang Z, Vihma T, Johansson M, Bian L, Li Z and Wu H (2008b) Model experiments on snow and ice
425 thermodynamics in the Arctic Ocean with CHINARE 2003 data. *Journal of Geophysical Research*, **113**, C09020
426 (doi: 10.1029/2007JC004654)
- 427 Cheng B, Mäkynen M, Similä M, Rontu L and Vihma T (2013) Modelling snow and ice thickness in the coastal Kara
428 Sea, Russian Arctic. *Annals of Glaciology*, **54**, 105–113 (doi: 10.3189/2013AoG62A180)
- 429 Clemens-Sewall D, Polashenski C, Perovich D and Webster MA (2024) The importance of sub-meter-scale snow
430 roughness on conductive heat flux of Arctic sea ice. *Journal of Glaciology*, 1–6 (doi: 10.1017/jog.2023.105)
- 431 Crameri F (2023) Scientific colour maps (doi: 10.5281/ZENODO.1243862)
- 432 Crameri F, Shephard GE and Heron PJ (2020) The misuse of colour in science communication. *Nature Communica-*
433 *tions*, **11**(1) (doi: 10.1038/s41467-020-19160-7)
- 434 DiGirolamo N, Parkinson C, Cavalieri D, Gloersen P and Zwally H (2022) Sea Ice Concentrations from Nimbus-7
435 SMMR and DMSP SSM/I-SSMIS Passive Microwave Data, Version 2 (doi: 10.5067/MPYG15WAA4WX), ac-
436 cessed: 2 April 2023
- 437 Gelaro R, McCarty W, Suárez MJ, Todling R, Molod A, Takacs L, Randles CA, Darmenov A, Bosilovich MG, Reichle
438 R, Wargan K, Coy L, Cullather R, Draper C, Akella S, Buchard V, Conaty A, da Silva AM, Gu W, Kim GK,
439 Koster R, Lucchesi R, Merkova D, Nielsen JE, Partyka G, Pawson S, Putman W, Rienecker M, Schubert SD,
440 Sienkiewicz M and Zhao B (2017) The Modern-Era Retrospective Analysis for Research and Applications, Version
441 2 (MERRA-2). *Journal of Climate*, **30**, 5419–5454 (doi: 10.1175/JCLI-D-16-0758.1)

- 442 Giles K, Laxon S, Wingham D, Wallis D, Krabill W, Leuschen C, McAdoo D, Manizade S and Raney R (2007)
443 Combined airborne laser and radar altimeter measurements over the Fram Strait in May 2002. *Remote Sensing of*
444 *Environment*, **111**, 182–194 (doi: 10.1016/j.rse.2007.02.037)
- 445 Global Modeling And Assimilation Office (GMAO) (2015a) MERRA-2 tavg1_2d_flux_Nx: 2d, 1-Hourly, Time-
446 Averaged, Single-Level, Assimilation, Surface Flux Diagnostics V5.12.4 (doi: 10.5067/7MCPBJ41Y0K6), accessed:
447 7 January 2023
- 448 Global Modeling And Assimilation Office (GMAO) (2015b) MERRA-2 tavg1_2d_slv_Nx: 2d, 1-Hourly, Time-
449 Averaged, Single-Level, Assimilation, Single-Level Diagnostics V5.12.4 (doi: 10.5067/VJAFPLI1CSIV), accessed:
450 7 January 2023
- 451 Granskog MA, Rösel A, Dodd PA, Divine D, Gerland S, Martma T and Leng MJ (2017) Snow contribution to first-
452 year and second-year Arctic sea ice mass balance north of Svalbard. *Journal of Geophysical Research: Oceans*,
453 **122**, 2539–2549 (doi: 10.1002/2016JC012398)
- 454 Hersbach H, Bell B, Berrisford P, Hirahara S, Horányi A, Muñoz-Sabater J, Nicolas J, Peubey C, Radu R, Schepers
455 D, Simmons A, Soci C, Abdalla S, Abellan X, Balsamo G, Bechtold P, Biavati G, Bidlot J, Bonavita M, Chiara
456 G, Dahlgren P, Dee D, Diamantakis M, Dragani R, Flemming J, Forbes R, Fuentes M, Geer A, Haimberger L,
457 Healy S, Hogan RJ, Hólm E, Janisková M, Keeley S, Laloyaux P, Lopez P, Lupu C, Radnoti G, Rosnay P, Rozum
458 I, Vamborg F, Villaume S and Thépaut J (2020) The ERA5 global reanalysis. *Quarterly Journal of the Royal*
459 *Meteorological Society*, **146**, 1999–2049 (doi: 10.1002/qj.3803)
- 460 Itkin P, Hendricks S, Webster MA, von Albedyll L, Arndt S, Divine D, Jaggi M, Oggier M, Raphael I, Ricker R, Rohde
461 J, Schneebeli M and Liston GE (2023) Sea ice and snow characteristics from year-long transects at the MOSAiC
462 Central Observatory. *Elementa: Science of the Anthropocene*, **11**(1), 00048 (doi: 10.1525/elementa.2022.00048)
- 463 Jutila A, King J, Ricker R, Hendricks S, Helm V, Binder T and Haas C (2021a) Airborne snow depth on sea ice during
464 the IceBird Winter 2019 campaign in the Arctic Ocean, Version 1 (doi: 10.1594/PANGAEA.932790), accessed: 18
465 July 2023
- 466 Jutila A, King J, Ricker R, Hendricks S, Helm V, Binder T and Herber A (2021b) Airborne snow depth on sea
467 ice during the PAMARCMIP2017 campaign in the Arctic Ocean, Version 1 (doi: 10.1594/PANGAEA.932668),
468 accessed: 18 July 2023
- 469 Jutila A, Hendricks S, Ricker R, von Albedyll L, Krumpfen T and Haas C (2022a) Retrieval and parameterisation
470 of sea-ice bulk density from airborne multi-sensor measurements. *The Cryosphere*, **16**, 259–275 (doi: 10.5194/
471 tc-16-259-2022)

- 472 Jutila A, King J, Paden J, Ricker R, Hendricks S, Polashenski C, Helm V, Binder T and Haas C (2022b) High-
473 Resolution Snow Depth on Arctic Sea Ice From Low-Altitude Airborne Microwave Radar Data. *IEEE Transactions*
474 *on Geoscience and Remote Sensing*, **60**, 4300716 (doi: 10.1109/TGRS.2021.3063756)
- 475 Jutila A, Hendricks S, Ricker R, von Albedyll L and Haas C (2024a) Airborne sea ice parameters during the IceBird
476 Winter 2019 campaign in the Arctic Ocean, Version 2 (doi: 10.1594/PANGAEA.966057), accessed: 5 March 2024
- 477 Jutila A, Hendricks S, Ricker R, von Albedyll L and Haas C (2024b) Airborne sea ice parameters during the PA-
478 MARCMIP2017 campaign in the Arctic Ocean, Version 2 (doi: 10.1594/PANGAEA.966009), accessed: 5 March
479 2024
- 480 Kurtz NT and Farrell SL (2011) Large-scale surveys of snow depth on Arctic sea ice from Operation IceBridge.
481 *Geophysical Research Letters*, **38**(20), L20505 (doi: 10.1029/2011gl049216)
- 482 Kurtz NT, Farrell SL, Studinger M, Galin N, Harbeck JP, Lindsay R, Onana VD, Panzer B and Sonntag JG (2013)
483 Sea ice thickness, freeboard, and snow depth products from Operation IceBridge airborne data. *The Cryosphere*,
484 **7**(4), 1035–1056 (doi: 10.5194/tc-7-1035-2013)
- 485 Kurtz NT, Studinger M, Harbeck J, DePaul Onana V and Yi D (2015) IceBridge L4 Sea Ice Freeboard, Snow Depth,
486 and Thickness, Version 1 (doi: 10.5067/G519SHCKWQV6), accessed: 18 July 2023
- 487 Kurtz NT, Studinger M, Harbeck J, DePaul Onana V and Yi D (2016) IceBridge Sea Ice Freeboard, Snow Depth,
488 and Thickness Quick Look, Version 1 (doi: 10.5067/GRIXZ91DE0L9), accessed: 18 July 2023
- 489 Kwok R and Cunningham GF (2008) ICESat over Arctic sea ice: Estimation of snow depth and ice thickness. *Journal*
490 *of Geophysical Research*, **113**, C08010 (doi: 10.1029/2008JC004753)
- 491 Kwok R, Cunningham GF, Wensnahan M, Rigor I, Zwally HJ and Yi D (2009) Thinning and volume loss of the Arctic
492 Ocean sea ice cover: 2003–2008. *Journal of Geophysical Research*, **114**, C07005 (doi: 10.1029/2009JC005312)
- 493 Landy JC, Petty AA, Tsamados M and Stroeve JC (2020) Sea Ice Roughness Overlooked as a Key Source of
494 Uncertainty in CryoSat-2 Ice Freeboard Retrievals. *Journal of Geophysical Research: Oceans*, **125**, e2019JC015820
495 (doi: 10.1029/2019JC015820)
- 496 Landy JC, Dawson GJ, Tsamados M, Bushuk M, Stroeve JC, Howell SEL, Krumpfen T, Babb DG, Komarov AS,
497 Heorton HDBS, Belter HJ and Aksenov Y (2022) A year-round satellite sea-ice thickness record from CryoSat-2.
498 *Nature*, **609**(7927), 517–522 (doi: 10.1038/s41586-022-05058-5)
- 499 Launiainen J and Cheng B (1998) Modelling of ice thermodynamics in natural water bodies. *Cold Regions Science*
500 *and Technology*, **27**, 153–178 (doi: 10.1016/S0165-232X(98)00009-3)

- 501 Laxon S, Peacock N and Smith D (2003) High interannual variability of sea ice thickness in the Arctic region. *Nature*,
502 **425**, 947–950 (doi: 10.1038/nature02050)
- 503 Ledley TS (1991) Snow on sea ice: Competing effects in shaping climate. *Journal of Geophysical Research: Atmo-*
504 *spheres*, **96**(D9), 17195–17208 (doi: 10.1029/91jd01439)
- 505 Leppäranta M (1983) A Growth Model for Black Ice, Snow Ice and Snow Thickness in Subarctic Basins. *Hydrology*
506 *Research*, **14**, 59–70 (doi: 10.2166/nh.1983.0006)
- 507 Liston GE and Elder K (2006a) A Distributed Snow-Evolution Modeling System (SnowModel). *Journal of Hydrom-*
508 *eteorology*, **7**, 1259–1276 (doi: 10.1175/JHM548.1)
- 509 Liston GE and Elder K (2006b) A Meteorological Distribution System for High-Resolution Terrestrial Modeling
510 (MicroMet). *Journal of Hydrometeorology*, **7**(2), 217–234 (doi: 10.1175/JHM486.1)
- 511 Liston GE, Polashenski C, Rösel A, Itkin P, King J, Merkouriadi I and Haapala J (2018) A Distributed Snow-
512 Evolution Model for Sea-Ice Applications (SnowModel). *Journal of Geophysical Research: Oceans*, **123**, 3786–3810
513 (doi: 10.1002/2017JC013706)
- 514 Liston GE, Itkin P, Stroeve J, Tschudi M, Stewart JS, Pedersen SH, Reinking AK and Elder K (2020a) A La-
515 grangian Snow-Evolution System for Sea-Ice Applications (SnowModel-LG): Part I — Model Description. *Journal*
516 *of Geophysical Research: Oceans*, **125**, e2019JC015913 (doi: 10.1029/2019JC015913)
- 517 Liston GE, Stroeve J and Itkin P (2020b) Lagrangian Snow Distributions for Sea-Ice Applications (doi: 10.5067/
518 27A0P5M6LZBI)
- 519 Macfarlane AR, Schneebeli M, Dacic R, Tavri A, Immerz A, Polashenski C, Krampe D, Clemens-Sewall D, Wagner
520 DN, Perovich DK, Henna-Reetta H, Raphael I, Matero I, Regnery J, Smith MM, Nicolaus M, Jaggi M, Oggier
521 M, Webster MA, Lehning M, Kolabutin N, Itkin P, Naderpour R, Pirazzini R, Hämmerle S, Arndt S and Fons S
522 (2023) A Database of Snow on Sea Ice in the Central Arctic Collected during the MOSAiC expedition. *Scientific*
523 *Data*, **10**, 398 (doi: 10.1038/s41597-023-02273-1)
- 524 MacGregor JA, Boisvert LN, Medley B, Petty AA, Harbeck JP, Bell RE, Blair JB, Blanchard-Wrigglesworth E,
525 Buckley EM, Christoffersen MS, Cochran JR, Csathó BM, Marco EL, Dominguez RT, Fahnestock MA, Farrell
526 SL, Gogineni SP, Greenbaum JS, Hansen CM, Hofton MA, Holt JW, Jezek KC, Koenig LS, Kurtz NT, Kwok R,
527 Larsen CF, Leuschen CJ, Locke CD, Manizade SS, Martin S, Neumann TA, Nowicki SM, Paden JD, Richter-Menge
528 JA, Rignot EJ, Rodríguez-Morales F, Siegfried MR, Smith BE, Sonntag JG, Studinger M, Tinto KJ, Truffer M,
529 Wagner TP, Woods JE, Young DA and Yungel JK (2021) The Scientific Legacy of NASA’s Operation IceBridge.
530 *Reviews of Geophysics*, **59**, e2020RG000712 (doi: 10.1029/2020RG000712)

- 531 Markus T, Neumann T, Martino A, Abdalati W, Brunt K, Csatho B, Farrell S, Fricker H, Gardner A, Harding D,
532 Jasinski M, Kwok R, Magruder L, Lubin D, Luthcke S, Morison J, Nelson R, Neuenschwander A, Palm S, Popescu
533 S, Shum C, Schutz BE, Smith B, Yang Y and Zwally J (2017) The Ice, Cloud, and land Elevation Satellite-2
534 (ICESat-2): Science requirements, concept, and implementation. *Remote Sensing of Environment*, **190**, 260–273
535 (doi: 10.1016/j.rse.2016.12.029)
- 536 Maslanik JA, Fowler C, Stroeve J, Drobot S, Zwally J, Yi D and Emery W (2007) A younger, thinner Arctic
537 ice cover: Increased potential for rapid, extensive sea-ice loss. *Geophysical Research Letters*, **34**, L24501 (doi:
538 10.1029/2007GL032043)
- 539 Massom RA, Eicken H, Haas C, Jeffries MO, Drinkwater MR, Sturm M, Worby AP, Wu X, Lytle VI, Ushio S, Morris
540 K, Reid PA, Warren SG and Allison I (2001) Snow on Antarctic sea ice. *Reviews of Geophysics*, **39**(3), 413–445
541 (doi: 10.1029/2000rg000085)
- 542 Maykut GA (1978) Energy exchange over young sea ice in the central Arctic. *Journal of Geophysical Research:*
543 *Oceans*, **83**(C7), 3646–3658 (doi: 10.1029/jc083ic07p03646)
- 544 Meier WN, Hovelsrud GK, van Oort BE, Key JR, Kovacs KM, Michel C, Haas C, Granskog MA, Gerland S, Perovich
545 DK, Makshtas A and Reist JD (2014) Arctic sea ice in transformation: A review of recent observed changes and
546 impacts on biology and human activity. *Reviews of Geophysics*, **52**, 185–217 (doi: 10.1002/2013RG000431)
- 547 Merkouriadi I, Cheng B, Graham RM, Rösel A and Granskog MA (2017) Critical Role of Snow on Sea Ice
548 Growth in the Atlantic Sector of the Arctic Ocean. *Geophysical Research Letters*, **44**, 10479–10485 (doi:
549 10.1002/2017GL075494)
- 550 Merkouriadi I, Liston GE, Graham RM and Granskog MA (2020) Quantifying the Potential for Snow-Ice Formation
551 in the Arctic Ocean. *Geophysical Research Letters*, **47**, e2019GL085020 (doi: 10.1029/2019GL085020)
- 552 National Information Standards Organization (NISO) (2022) ANSI/NISO Z39.104-2022, CRediT, Contributor Roles
553 Taxonomy (doi: 10.3789/ansi.niso.z39.104-2022)
- 554 Perovich D, Polashenski C, Arntsen A and Stwertka C (2017) Anatomy of a late spring snowfall on sea ice. *Geophysical*
555 *Research Letters*, **44**(6), 2802–2809 (doi: 10.1002/2016gl071470)
- 556 Petty AA, Webster M, Boisvert L and Markus T (2018) The NASA Eulerian Snow on Sea Ice Model (NESOSIM)
557 v1.0: initial model development and analysis. *Geoscientific Model Development*, **11**, 4577–4602 (doi: 10.5194/
558 gmd-11-4577-2018)
- 559 Preußner A, Nicolaus M and Hoppmann M (2024, in review) Snow depth, sea ice thickness and interface temperatures
560 derived from measurements of SIMBA buoys deployed in the Arctic Ocean and Southern Ocean between 2012 and
561 2023. Accessed: 18 November 2024 at <https://doi.pangaea.de/10.1594/PANGAEA.973193>

- 562 Pringle DJ, Eicken H, Trodahl HJ and Backstrom LGE (2007) Thermal conductivity of landfast Antarctic and Arctic
563 sea ice. *Journal of Geophysical Research*, **112**, C04017 (doi: 10.1029/2006JC003641)
- 564 Provost C, Sennéchaël N, Miguet J, Itkin P, Rösel A, Koenig Z, Villacieros-Robineau N and Granskog MA (2017)
565 Observations of flooding and snow-ice formation in a thinner Arctic sea-ice regime during the N-ICE 2015 campaign:
566 Influence of basal ice melt and storms. *Journal of Geophysical Research: Oceans*, **122**, 7115–7134 (doi: 10.1002/
567 2016JC012011)
- 568 Radionov VF, Bryazgin NN and Alexandrov EI (1997) The Snow Cover of the Arctic Basin. Technical Report
569 APL-UW TR 9701, Applied Physics Laboratory, University of Washington, Seattle, Washington
- 570 Saloranta TM (2000) Modeling the evolution of snow, snow ice and ice in the Baltic Sea. *Tellus A: Dynamic Meteo-*
571 *rology and Oceanography*, **52**, 93–108 (doi: 10.3402/tellusa.v52i1.12255)
- 572 Stroeve JC, Markus T, Boisvert L, Miller J and Barrett A (2014) Changes in Arctic melt season and implications
573 for sea ice loss. *Geophysical Research Letters*, **41**, 1216–1225 (doi: 10.1002/2013GL058951)
- 574 Stroeve JC, Liston GE, Buzzard S, Zhou L, Mallett R, Barrett A, Tschudi M, Tsamados M, Itkin P and Stewart
575 JS (2020) A Lagrangian Snow Evolution System for Sea Ice Applications (SnowModel-LG): Part II — Analyses.
576 *Journal of Geophysical Research: Oceans*, **125**, e2019JC015900 (doi: 10.1029/2019JC015900)
- 577 Sturm M, Holmgren J and Perovich DK (2002) Winter snow cover on the sea ice of the Arctic Ocean at the Surface
578 Heat Budget of the Arctic Ocean (SHEBA): Temporal evolution and spatial variability. *Journal of Geophysical*
579 *Research: Oceans*, **107**(C10) (doi: 10.1029/2000jc000400)
- 580 Thielke L, Fuchs N, Spreen G, Tremblay B, Birnbaum G, Huntemann M, Hutter N, Itkin P, Jutila A and Webster MA
581 (2023) Preconditioning of Summer Melt Ponds From Winter Sea Ice Surface Temperature. *Geophysical Research*
582 *Letters*, **50**(4), e2022GL101493 (doi: 10.1029/2022gl101493)
- 583 Tschudi M, Meier WN, Stewart JS, Fowler C and Maslanik J (2019) Polar Pathfinder Daily 25 km EASE-Grid Sea
584 Ice Motion Vectors, Version 4 (doi: 10.5067/INAWUWO7QH7B), accessed: 20 March 2023
- 585 Tschudi M, Meier WN and Stewart JS (2020) An enhancement to sea ice motion and age products at the National
586 Snow and Ice Data Center (NSIDC). *The Cryosphere*, **14**(5), 1519–1536 (doi: 10.5194/tc-14-1519-2020)
- 587 Wang C, Cheng B, Wang K, Gerland S and Pavlova O (2015) Modelling snow ice and superimposed ice on landfast
588 sea ice in Kongsfjorden, Svalbard. *Polar Research*, **34**, 20828 (doi: 10.3402/polar.v34.20828)
- 589 Warren SG, Rigor IG, Untersteiner N, Radionov VF, Bryazgin NN, Aleksandrov YI and Colony R (1999) Snow Depth
590 on Arctic Sea Ice. *Journal of Climate*, **12**, 1814–1829 (doi: 10.1175/1520-0442(1999)012<1814:SDOASI>2.0.CO;2)

- 591 Webster MA, Rigor IG, Perovich DK, Richter-Menge JA, Polashenski CM and Light B (2015) Seasonal evolution
592 of melt ponds on Arctic sea ice. *Journal of Geophysical Research: Oceans*, **120**(9), 5968–5982 (doi: 10.1002/
593 2015jc011030)
- 594 Webster MA, DuVivier AK, Holland MM and Bailey DA (2021) Snow on Arctic Sea Ice in a Warming Climate as Sim-
595 ulated in CESM. *Journal of Geophysical Research: Oceans*, **126**(1), e2020JC016308 (doi: 10.1029/2020jc016308)
- 596 Webster MA, Riihelä A, Kacimi S, Ballinger TJ, Blanchard-Wrigglesworth E, Parker CL and Boisvert L (2024)
597 Summer snow on Arctic sea ice modulated by the Arctic Oscillation. *Nature Geoscience*, **17**(10), 995–1002 (doi:
598 10.1038/s41561-024-01525-y)
- 599 Zampieri L, Clemens-Sewall D, Sledd A, Hutter N and Holland M (2024) Modeling the Winter Heat Conduction
600 Through the Sea Ice System During MOSAiC. *Geophysical Research Letters*, **51**(8), e2023GL106760 (doi: 10.1029/
601 2023gl106760)
- 602 Zuo H, Balmaseda MA, Tietsche S, Mogensen K and Mayer M (2019) The ECMWF operational ensemble reanalysis–
603 analysis system for ocean and sea ice: a description of the system and assessment. *Ocean Science*, **15**(3), 779–808
604 (doi: 10.5194/os-15-779-2019)
- 605 Zygmuntowska M, Rampal P, Ivanova N and Smedsrud LH (2014) Uncertainties in Arctic sea ice thickness and
606 volume: new estimates and implications for trends. *The Cryosphere*, **8**, 705–720 (doi: 10.5194/tc-8-705-2014)

607 **A APPENDIX – NASA OIB SURVEY STATISTICS**

Table 2. Statistics of the 99 NASA Operation IceBridge survey flights over the western Arctic Ocean in 2009–2019 (Fig. 1) used in this study, where L is the total length of the survey flight, $\bar{h}_{s,\text{level}}$ is the average snow depth on level ice, $\bar{h}_{s,\text{deformed}}$ is the average snow depth on deformed ice, $\bar{h}_{s,\text{all}}$ is the average snow depth of the entire survey flight including all ice types, $\frac{\bar{h}_{s,\text{level}}}{\bar{h}_{s,\text{deformed}}}$ is the fraction of the average snow depth on level ice to the average snow depth on deformed ice, f_{level} is the level ice fraction of the survey flight, $f_{V_{s,\text{level}}}$ is the fraction of snow volume on level ice, f_{MYI} is the fraction of multi-year ice (MYI), and f_{NaN} is the fraction of missing snow depth data

Date	L (km)	$\bar{h}_{s,\text{level}}$ (m)	$\bar{h}_{s,\text{deformed}}$ (m)	$\bar{h}_{s,\text{all}}$ (m)	$\frac{\bar{h}_{s,\text{level}}}{\bar{h}_{s,\text{deformed}}}$	f_{level}	$f_{V_{s,\text{level}}}$	f_{MYI}	f_{NaN}
2009-04-02	2332	0.207	0.320	0.313	0.647	0.066	0.044	0.748	0.383
2009-04-05	2556	0.228	0.220	0.220	1.037	0.030	0.031	0.948	0.165
2009-04-21	631	0.235	0.356	0.351	0.660	0.036	0.024	0.894	0.423
2009-04-25	3050	0.168	0.277	0.273	0.605	0.038	0.024	0.341	0.783
2010-03-23	2660	0.267	0.334	0.333	0.799	0.014	0.011	0.998	0.362
2010-03-26	2822	0.107	0.240	0.232	0.443	0.058	0.027	0.858	0.425
2010-04-02	3039	0.099	0.135	0.130	0.733	0.142	0.108	0.743	0.145
2010-04-05	2796	0.126	0.228	0.222	0.552	0.062	0.035	0.952	0.321
2010-04-12	2570	0.162	0.285	0.280	0.568	0.044	0.026	0.986	0.313
2010-04-19	2028	0.152	0.229	0.223	0.660	0.082	0.055	0.982	0.140
2010-04-20	1733	0.144	0.257	0.252	0.560	0.045	0.026	0.957	0.192
2010-04-21	1885	0.107	0.249	0.238	0.432	0.074	0.033	0.985	0.496
2011-03-16	1126	0.155	0.200	0.198	0.775	0.051	0.040	0.884	0.115
2011-03-17	1869	0.175	0.227	0.226	0.771	0.029	0.022	0.791	0.074
2011-03-18	1779	0.188	0.234	0.233	0.805	0.013	0.011	0.970	0.121
2011-03-22	1159	0.142	0.210	0.207	0.676	0.041	0.028	0.949	0.058
2011-03-23	1402	0.084	0.123	0.111	0.683	0.315	0.239	1.000	0.158
2011-03-25	2248	0.228	0.199	0.200	1.142	0.007	0.008	0.929	0.135
2011-03-26	2247	0.201	0.245	0.244	0.821	0.021	0.018	0.980	0.126
2011-03-28	2669	0.150	0.237	0.235	0.631	0.023	0.014	0.769	0.202

(Continued)

Date	L (km)	$\bar{h}_{s,level}$ (m)	$\bar{h}_{s,deformed}$ (m)	$\bar{h}_{s,all}$ (m)	$\frac{\bar{h}_{s,level}}{\bar{h}_{s,deformed}}$	f_{level}	$f_{V_{s,level}}$	f_{MYI}	f_{NaN}
2012-03-14	2399	0.191	0.221	0.221	0.866	0.001	0.001	0.969	0.408
2012-03-15	2422	0.117	0.152	0.150	0.773	0.064	0.050	0.951	0.267
2012-03-16	2580	0.112	0.124	0.124	0.907	0.030	0.027	0.960	0.354
2012-03-17	2171	0.107	0.137	0.136	0.782	0.050	0.040	0.937	0.271
2012-03-19	2187	0.313	0.258	0.258	1.214	0.001	0.001	0.930	0.259
2012-03-21	2340	0.182	0.247	0.247	0.734	0.012	0.009	0.769	0.416
2012-03-22	2043	0.180	0.241	0.241	0.745	0.012	0.009	0.917	0.349
2012-03-23	2453	0.206	0.257	0.257	0.803	0.004	0.004	0.942	0.343
2012-03-26	1473	0.225	0.241	0.241	0.933	0.006	0.005	1.000	0.702
2012-03-27	1878	0.196	0.302	0.301	0.651	0.007	0.004	0.994	0.424
2012-03-28	2473	0.304	0.230	0.230	1.323	0.006	0.008	0.647	0.599
2012-03-29	2113	0.348	0.324	0.324	1.074	0.009	0.010	0.987	0.210
2012-04-02	2270	0.206	0.281	0.281	0.732	0.004	0.003	0.776	0.455
2012-04-10	1809	0.065	0.266	0.265	0.244	0.007	0.002	0.863	0.657
2013-03-21	2521	0.133	0.206	0.198	0.647	0.109	0.073	0.983	0.374
2013-03-22	2481	0.109	0.109	0.109	1.001	0.247	0.247	0.986	0.516
2013-03-23	2325	0.114	0.197	0.171	0.580	0.317	0.213	0.958	0.264
2013-03-24	2380	0.116	0.138	0.129	0.845	0.411	0.371	0.949	0.233
2013-03-26	2234	0.197	0.270	0.268	0.730	0.029	0.021	0.913	0.169
2013-03-27	2464	0.140	0.365	0.348	0.385	0.074	0.030	0.684	0.292
2013-04-22	2007	0.187	0.306	0.298	0.611	0.061	0.038	0.967	0.247
2013-04-24	2400	0.206	0.300	0.293	0.686	0.071	0.049	0.804	0.400
2013-04-25	1739	0.192	0.315	0.307	0.610	0.062	0.039	0.925	0.330
2014-03-12	1110	0.183	0.171	0.172	1.071	0.085	0.090	0.847	0.505
2014-03-13	1824	0.290	0.258	0.259	1.125	0.040	0.044	0.910	0.268
2014-03-14	2465	0.150	0.193	0.190	0.779	0.071	0.056	0.985	0.344
2014-03-15	2143	0.136	0.135	0.135	1.010	0.062	0.063	0.956	0.645
2014-03-17	2058	0.141	0.159	0.157	0.886	0.102	0.092	0.848	0.381

(Continued)

Date	L (km)	$\bar{h}_{s,level}$ (m)	$\bar{h}_{s,deformed}$ (m)	$\bar{h}_{s,all}$ (m)	$\frac{\bar{h}_{s,level}}{\bar{h}_{s,deformed}}$	f_{level}	$f_{V_{s,level}}$	f_{MYI}	f_{NaN}
2014-03-18	2386	0.129	0.145	0.144	0.894	0.059	0.053	0.946	0.563
2014-03-19	2354	0.135	0.150	0.149	0.896	0.090	0.082	0.954	0.435
2014-03-21	2225	0.301	0.253	0.253	1.187	0.005	0.006	1.000	0.412
2014-03-24	1150	0.274	0.220	0.223	1.241	0.055	0.068	0.678	0.455
2014-03-25	2232	0.065	0.108	0.107	0.602	0.027	0.016	0.014	0.422
2014-03-26	2204	0.396	0.267	0.268	1.485	0.008	0.011	0.972	0.332
2014-03-28	1495	0.250	0.287	0.286	0.872	0.015	0.013	0.960	0.289
2014-03-31	1577	0.093	0.299	0.295	0.313	0.020	0.006	0.886	0.306
2014-04-03	2994	0.216	0.277	0.276	0.779	0.019	0.015	0.955	0.209
2014-04-28	2115	0.244	0.279	0.278	0.877	0.018	0.016	0.889	0.238
2015-03-19	937	0.214	0.299	0.296	0.714	0.045	0.032	0.699	0.519
2015-03-24	1378	0.255	0.307	0.305	0.830	0.041	0.034	0.822	0.458
2015-03-25	2275	0.170	0.297	0.291	0.571	0.050	0.029	0.917	0.259
2015-03-26	2177	0.155	0.247	0.243	0.628	0.046	0.029	0.974	0.351
2015-03-27	2083	0.125	0.246	0.238	0.509	0.067	0.035	0.955	0.501
2015-03-29	2466	0.115	0.170	0.165	0.679	0.101	0.071	0.923	0.420
2015-03-30	2134	0.100	0.180	0.172	0.555	0.106	0.062	0.867	0.462
2015-04-01	1646	0.157	0.379	0.378	0.414	0.004	0.002	1.000	0.276
2015-04-03	1503	0.228	0.333	0.330	0.685	0.022	0.015	0.952	0.306
2016-04-20	2536	0.107	0.285	0.280	0.375	0.029	0.011	0.952	0.652
2016-04-21	2337	0.108	0.156	0.154	0.692	0.039	0.027	0.793	0.749
2016-04-29	2079	0.340	0.343	0.343	0.990	0.015	0.014	0.843	0.656
2016-05-03	1749	0.290	0.339	0.339	0.855	0.003	0.003	0.782	0.599
2016-05-04	1724	0.252	0.307	0.306	0.823	0.007	0.006	0.808	0.668
2017-03-09	2146	0.154	0.279	0.269	0.552	0.082	0.047	0.950	0.158
2017-03-10	2368	0.167	0.225	0.220	0.740	0.087	0.066	0.959	0.271
2017-03-11	2193	0.106	0.181	0.159	0.585	0.292	0.195	0.994	0.168
2017-03-12	2262	0.105	0.133	0.123	0.785	0.364	0.310	0.970	0.246

(Continued)

Date	L (km)	$\bar{h}_{s,level}$ (m)	$\bar{h}_{s,deformed}$ (m)	$\bar{h}_{s,all}$ (m)	$\frac{\bar{h}_{s,level}}{\bar{h}_{s,deformed}}$	f_{level}	$f_{V_{s,level}}$	f_{MYI}	f_{NaN}
2017-03-14	2378	0.193	0.247	0.236	0.782	0.200	0.164	0.881	0.049
2017-03-20	2300	0.183	0.280	0.272	0.651	0.080	0.053	0.956	0.232
2017-03-23	2096	0.172	0.390	0.380	0.441	0.045	0.020	1.000	0.317
2017-03-24	1233	0.141	0.333	0.328	0.424	0.025	0.011	0.980	0.212
2017-04-03	769	0.037	0.241	0.194	0.153	0.231	0.044	0.677	0.564
2017-04-05	2635	0.175	0.252	0.246	0.696	0.075	0.053	0.976	0.382
2017-04-06	1703	0.097	0.169	0.149	0.577	0.273	0.178	0.719	0.287
2017-04-07	2469	0.123	0.290	0.282	0.425	0.046	0.020	0.927	0.306
2017-04-11	2182	0.187	0.300	0.292	0.623	0.066	0.042	0.925	0.201
2017-04-19	1690	0.145	0.255	0.241	0.571	0.121	0.073	0.931	0.186
2018-03-22	1914	0.117	0.265	0.256	0.442	0.066	0.030	0.814	0.264
2018-04-03	1446	0.110	0.230	0.210	0.476	0.164	0.085	0.894	0.381
2018-04-04	2186	0.178	0.325	0.316	0.546	0.064	0.036	0.922	0.174
2018-04-06	2662	0.177	0.300	0.286	0.590	0.113	0.070	0.971	0.306
2018-04-07	2302	0.143	0.227	0.212	0.629	0.174	0.117	0.934	0.370
2018-04-08	2163	0.165	0.240	0.233	0.687	0.093	0.066	0.991	0.637
2018-04-14	2403	0.075	0.275	0.222	0.275	0.265	0.090	0.944	0.314
2018-04-16	2449	0.087	0.353	0.326	0.246	0.100	0.027	0.933	0.154
2019-04-06	1953	0.210	0.366	0.360	0.574	0.039	0.023	0.890	0.202
2019-04-12	1548	0.164	0.218	0.213	0.752	0.092	0.071	1.000	0.061
2019-04-19	1184	0.281	0.323	0.321	0.872	0.045	0.039	0.989	0.070
2019-04-20	1599	0.180	0.353	0.340	0.510	0.078	0.042	0.838	0.306
2019-04-22	743	0.241	0.267	0.266	0.903	0.044	0.040	0.978	0.063
min	631	0.037	0.108	0.107	0.153	0.001	0.001	0.014	0.049
mean	2062	0.174	0.249	0.243	0.714	0.074	0.051	0.894	0.336
max	3050	0.396	0.390	0.380	1.485	0.411	0.371	1.000	0.783

Supplementary material to the manuscript “Investigating snow sinks on level sea ice: A case study in the western Arctic”

Ioanna MERKOURIADI¹, Arttu JUTILA¹, Glen E. LISTON², Andreas PREUSSER^{3,4},
and Melinda A. WEBSTER⁵

¹*Finnish Meteorological Institute (FMI), Helsinki, Finland*

²*Cooperative Institute for Research in the Atmosphere (CIARA), Colorado State University, Fort Collins, CO,
USA*

³*Alfred-Wegener-Institut, Helmholtz-Zentrum für Polar- und Meeresforschung (AWI), Bremerhaven,
Germany*

⁴*Present address: German Space Agency at DLR, Bonn, Germany*

⁵*Polar Science Center (PSC), Applied Physics Laboratory, University of Washington, Seattle, WA, USA*

Correspondence: ioanna.merkouriadi@fmi.fi

Contents of this file

1. Text S1 to S2
2. Figure S1
3. Table S1

Introduction

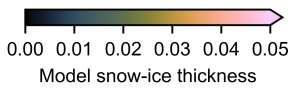
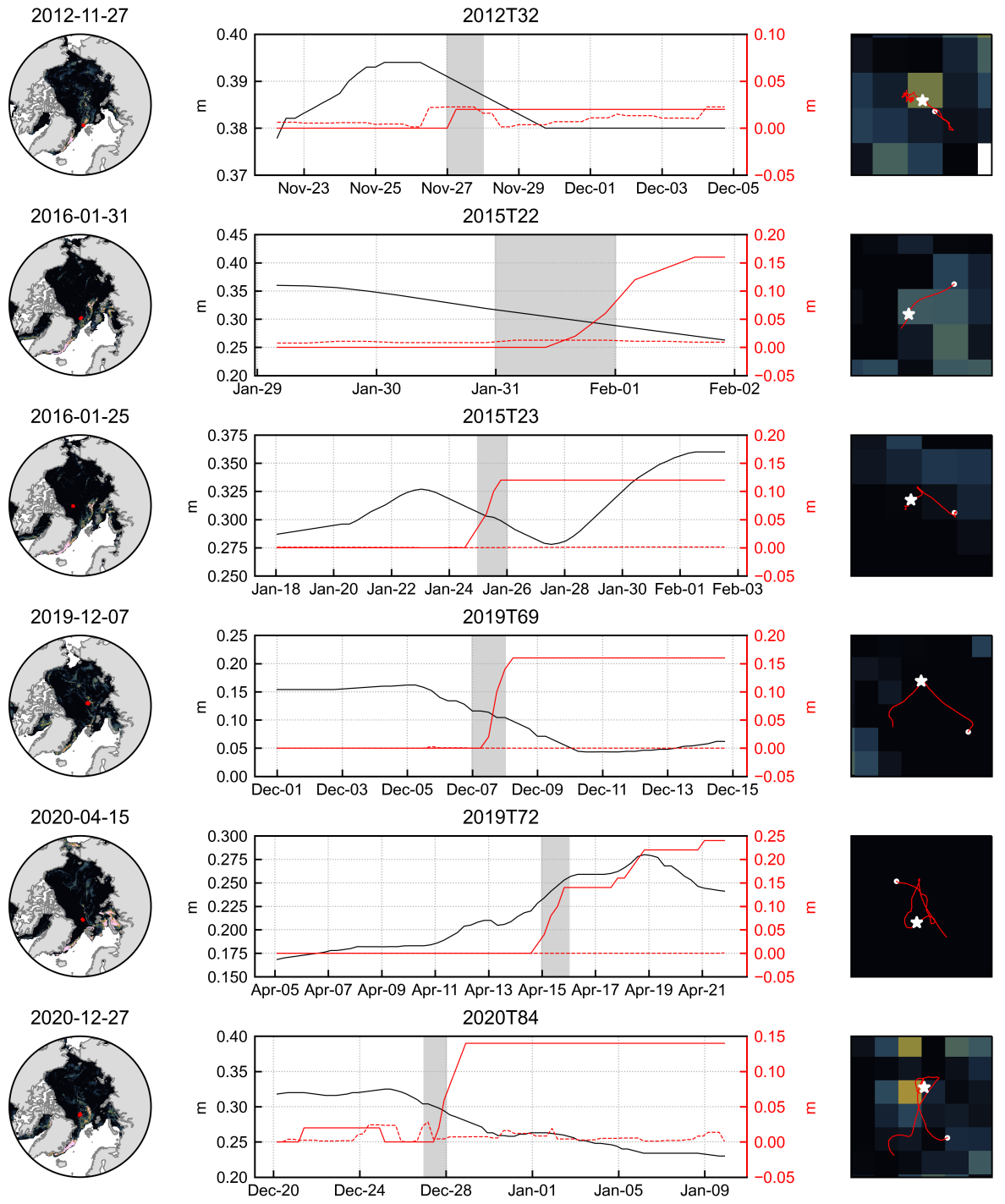
The supplementary material includes two short texts (S1–S2) explaining one table (S1) and one figure (S1).

Text S1. Model parametrization. Table S1 is descriptive, and it includes the HIGHTSI model parameterization used in this study.

Text S2. Snow-ice detection with buoys. We evaluated temperature profile and heating cycle data from thermistor strings of Snow Ice Mass Balance Apparatus (SIMBA) buoys (Jackson and others, 2013) deployed in the Arctic in 2012–2020 to detect flooding (Preußner and others, 2024). Changes in thermal diffusivity, temperature, and heat propagation distinguish the temporal evolution of different layers and their thicknesses (Provost and others, 2017; Preußner and others, 2023). Figure S1 shows a summary of SIMBA buoy data, where we examined wintertime snow-ice formation. The height change of the snow/ice interface shows a shift upward together with a decrease in snow depth at the presence of modeled snow-ice formation. Decrease in modeled snow-ice thickness is due to the nearest-neighbour method of extracting the closest gridded model data based on the sub-daily drift track data of the SIMBA buoys.

Table S1: Model parameters and constants used in this study.

Parameter	Value	Remarks/Source
Extinction coefficient of sea ice (k_i)	1.5–17 m ⁻¹	adopted from the paper by Grenfell and Maykut (1977)
Extinction coefficient of snow (k_s)	15–25 m ⁻¹	Perovich (1996)
Surface albedo ($\alpha_{s,i}$)	Time dependent	Briegleb and others (2004)
Freezing point (T_f)	-1.8 °C	
Sea ice volumetric heat capacity (ρc_i)	Function of T_i, s_i	Maykut and Untersteiner (1971)
Heat capacity of ice (c_i)	2093 Jkg ⁻¹ K ⁻¹	
Latent heat of freezing (L_i)	0.33×10^6 Jkg ⁻¹	
Oceanic heat flux (F_w)	Time dependent	ECMWF; Zuo and others (2019)
Sea ice density (ρ_i)	910 kgm ⁻³	
Snow-ice density (ρ_{si})	850 kgm ⁻³	Wang and others (2015)
Slush density (ρ_{sl})	920 kgm ⁻³	Wang and others (2015)
Sea ice salinity (s_i)	1–6	Ice core measurement Granskog and others (2017)
Snow density (ρ_s)	Time dependent	Liston and others (2020)
Surface emissivity (e)	0.97	
Sea ice heat conductivity (k_{si})	Function of T_i, s_i	Pringle and others (2007)
Thermal conductivity of ice (k_i)	2.03 Wm ⁻²	Maykut and Untersteiner (1971)
Time step of model (t)	3 h	
Initial temperature in snow and ice	[-1.25 °C, -1.8 °C]	Cheng and others (2008)
Number of layers in the ice	20	
Number of layers in the snow	25	



— Buoy snow depth - - - - Model snow-ice thickness ☆ Identified flooding
 — Buoy snow/ice interface height change ○ Time series start

Figure S1: Evaluation of the snow-ice formation using Snow Ice Mass Balance Apparatus (SIMBA) buoys. The left panels show the pan-Arctic simulated snow-ice thickness with the buoy location marked with a red dot on the day of identified flooding events. The middle panels show the time series of the snow depth measured by the buoy (black solid line, left vertical axes), of the snow/ice interface height change derived from the buoy data (red solid line, right vertical axes), and of the modeled snow-ice thickness of the nearest grid cell (red dashed line, right vertical axes) around the time of identified flooding events. The buoy names are given as the titles. Note the varying scales of the axes, both left and right vertical axes as well as the horizontal time axes. The gray background indicates the day depicted in the maps. The right panels show the drift track of the buoys with the start of the middle panel time series marked with a white dot and the time of identified flooding with a white star. Note the varying scale: however, a single grid cell is always 25 km × 25 km.

References

- Briegleb B, Bitz C, Hunke E, Lipscomb W, Holland M, Schramm J and Moritz R (2004) Scientific Description of the Sea Ice Component in the Community Climate System Model, Version 3. Technical report, University Corporation for Atmospheric Research (doi: 10.5065/D6HH6H1P)
- Cheng B, Vihma T, Zhanhai Z, Zhijun L and Huiding W (2008) Snow and sea ice thermodynamics in the Arctic: Model validation and sensitivity study against SHEBA data. *Advances in Polar Science*, **19**, 108–122
- Granskog MA, Rösel A, Dodd PA, Divine D, Gerland S, Martma T and Leng MJ (2017) Snow contribution to first-year and second-year Arctic sea ice mass balance north of Svalbard. *Journal of Geophysical Research: Oceans*, **122**, 2539–2549 (doi: 10.1002/2016JC012398)
- Grenfell TC and Maykut GA (1977) The Optical Properties of Ice and Snow in the Arctic Basin. *Journal of Glaciology*, **18**, 445–463 (doi: 10.3189/S0022143000021122)
- Jackson K, Wilkinson J, Maksym T, Meldrum D, Beckers J, Haas C and Mackenzie D (2013) A novel and low-cost sea ice mass balance buoy. *Journal of Atmospheric and Oceanic Technology*, **30**, 2676–2688 (doi: 10.1175/JTECH-D-13-00058.1)
- Liston GE, Itkin P, Stroeve J, Tschudi M, Stewart JS, Pedersen SH, Reinking AK and Elder K (2020) A Lagrangian Snow-Evolution System for Sea-Ice Applications (SnowModel-LG): Part I — Model Description. *Journal of Geophysical Research: Oceans*, **125**, e2019JC015913 (doi: 10.1029/2019JC015913)
- Maykut GA and Untersteiner N (1971) Some results from a time-dependent thermodynamic model of sea ice. *Journal of Geophysical Research*, **76**, 1550–1575 (doi: 10.1029/JC076i006p01550)
- Perovich DK (1996) The optical properties of sea ice. Technical report, Cold Regions Research and Engineering Laboratory
- Preußner A, Nicolaus M and Hoppmann M (2024, in review) Snow depth, sea ice thickness and interface temperatures derived from measurements of SIMBA buoys deployed in the Arctic Ocean and Southern Ocean between 2012 and 2023. Accessed: 18 November 2024 at <https://doi.pangaea.de/10.1594/PANGAEA.973193>
- Preußner A, Krumpfen T and Nicolaus M (2023) Snow and ice thickness derived from sea ice mass balance buoys in the Transpolar Drift system (doi: 10.5281/zenodo.10623770), IGS Symposium on Sea Ice: Across Temporal and Spatial Scales, Bremerhaven, Germany
- Pringle DJ, Eicken H, Trodahl HJ and Backstrom LGE (2007) Thermal conductivity of land-fast Antarctic and Arctic sea ice. *Journal of Geophysical Research*, **112**, C04017 (doi: 10.1029/2006JC003641)

- Provost C, Sennéchaël N, Miguet J, Itkin P, Rösel A, Koenig Z, Villacieros-Robineau N and Granskog MA (2017) Observations of flooding and snow-ice formation in a thinner Arctic sea-ice regime during the N-ICE 2015 campaign: Influence of basal ice melt and storms. *Journal of Geophysical Research: Oceans*, **122**, 7115–7134 (doi: 10.1002/2016JC012011)
- Wang C, Cheng B, Wang K, Gerland S and Pavlova O (2015) Modelling snow ice and superimposed ice on landfast sea ice in Kongsfjorden, Svalbard. *Polar Research*, **34**, 20828 (doi: 10.3402/polar.v34.20828)
- Zuo H, Balmaseda MA, Tietsche S, Mogensen K and Mayer M (2019) The ECMWF operational ensemble reanalysis–analysis system for ocean and sea ice: a description of the system and assessment. *Ocean Science*, **15**(3), 779–808 (doi: 10.5194/os-15-779-2019)